Searches for supersymmetry using the M_{T2} variable in hadronic events produced in pp collisions at 8 TeV

The CMS collaboration

E-mail: cms-publication-committee-chair@cern.ch

ABSTRACT: Searches for supersymmetry (SUSY) are performed using a sample of hadronic events produced in 8 TeV pp collisions at the CERN LHC. The searches are based on the M_{T2} variable, which is a measure of the transverse momentum imbalance in an event. The data were collected with the CMS detector and correspond to an integrated luminosity of $19.5\,\mathrm{fb}^{-1}$. Two related searches are performed. The first is an inclusive search based on signal regions defined by the value of the M_{T2} variable, the hadronic energy in the event, the jet multiplicity, and the number of jets identified as originating from bottom quarks. The second is a search for a mass peak corresponding to a Higgs boson decaying to a bottom quark-antiquark pair, where the Higgs boson is produced as a decay product of a SUSY particle. For both searches, the principal backgrounds are evaluated with data control samples. No significant excess over the expected number of background events is observed, and exclusion limits on various SUSY models are derived.

Contents

1 Introduction

Searches for physics beyond the standard model (SM) based on final states with jets and large values of transverse momentum imbalance $\vec{p}_T^{\text{miss}}$ are sensitive to a broad class of new-physics models. Here, we report the results of such searches based on the M_{T2} variable [1]. The M_{T2} variable characterizes $\vec{p}_T^{\text{miss}}$ in events with two pair-produced heavy particles, each of which decays to at least one undetected particle, leading to $\vec{p}_T^{\text{miss}}$. An example is supersymmetry (SUSY) with R-parity conservation [2], in which pair-produced SUSY

particles each decay to SM particles and to a massive, neutral, weakly interacting lightest SUSY particle (LSP), which escapes without detection. The value of M_{T2} reflects the masses of the pair-produced particles, which are much lighter for SM background processes than expected for SUSY particles such as squarks and gluinos. The M_{T2} variable was previously used for top-quark mass measurements by the CDF and CMS experiments [3, 4], and for SUSY searches by the CMS [5, 6] and ATLAS [7–13] experiments.

This paper describes searches for physics beyond the SM performed using a data sample of pp collisions collected in 2012 at a centre-of-mass energy of 8 TeV with the CMS detector at the CERN LHC. The size of the sample, measured by its integrated luminosity, is $19.5\,\mathrm{fb}^{-1}$.

Two different M_{T2}-based searches are presented. The first search, called the inclusive-M_{T2} search, employs several signal regions defined by the number of jets (N_{j}), the number of tagged bottom-quark jets (N_{b}), the value of M_{T2}, and the hadronic energy in an event. This general search aims to cover a large variety of SUSY and other new-physics signatures. The second search, called the M_{T2}-Higgs search, is a specialized analysis targeting events with a Higgs boson produced in the decay of a heavy SUSY particle. The SM Higgs boson decays primarily to a bottom quark-antiquark ($b\bar{b}$) pair. For a large variety of SUSY models, the lightest Higgs boson (h boson) has SM properties, especially if the masses of all other SUSY Higgs bosons are much larger. In the M_{T2}-Higgs search, we therefore search for an excess of events at the SM Higgs boson mass of 125 GeV in the invariant mass distribution of b-tagged jet pairs.

The two searches rely on similar selection criteria for the M_{T2} variable to enhance the sensitivity to a potential SUSY signal and to reduce the background from SM multijet events to a minimal level. The remaining SM background consists mostly of Z+jets events where the Z boson decays to neutrinos, and W+jets and $t\bar{t}$ +jets events where one W boson decays leptonically. These backgrounds are mostly estimated by methods using data.

This analysis extends a previous CMS publication [5], based on pp collisions at 7 TeV, by exploiting a higher collision energy and a larger data sample. Alternative inclusive searches in hadronic final states based on the 8 TeV data sample are presented in refs. [14–18].

This paper is organized as follows. In section 2, the M_{T2} variable is defined. A description of the detector and trigger is given in section 3. The data sets and the general event selection procedures are discussed in section 4. Section 5 presents the analysis strategy for the inclusive-M_{T2} and M_{T2}-Higgs searches, and section 6 the background estimation method based on data control samples. A comparison between the observed numbers of events and the predicted background yields is presented for the two searches in section 7. Systematic uncertainties are discussed in section 8. The statistical procedures used to calculate exclusion limits on SUSY particles are presented in section 9, with the limits themselves presented in section 10. Section 11 contains a summary.

2 Definition of the M_{T2} variable and interpretation

The use of M_{T2} as a search variable is discussed in our previous publication [5]. Here, we recapitulate the most salient aspects. The kinematic mass variable M_{T2} was introduced as

a means to measure the mass of pair-produced particles in situations where both particles decay to a final state containing an undetected particle X of mass m_X. For each decay chain, the visible system is defined by the transverse momentum $\vec{p}_T^{\text{vis}(i)}$, transverse energy $E_T^{\text{vis}(i)}$, and mass $m^{\text{vis}(i)}$ ($i = 1, 2$) obtained by summing the four-momenta of all detected particles in the decay chain. The two visible systems are accompanied by the two undetected particles with unknown transverse momenta $\vec{p}_T^{X(i)}$. In analogy with the transverse mass used for the W boson mass determination [19], two transverse masses are defined for the two pair-produced particles:

$$(M_T^{(i)})^2 = (m^{\text{vis}(i)})^2 + m_X^2 + 2\left(E_T^{\text{vis}(i)} E_T^{X(i)} - \vec{p}_T^{\text{vis}(i)} \cdot \vec{p}_T^{X(i)}\right). \qquad (2.1)$$

If the correct values of m_X and $\vec{p}_T^{X(i)}$, $m^{\text{vis}(i)}$, and $\vec{p}_T^{\text{vis}(i)}$ are chosen, the transverse masses $M_T^{(i)}$ do not exceed the mass of the parent particles. The momenta $\vec{p}_T^{X(i)}$ of the unseen particles, however, are not experimentally accessible individually. Only their sum, the missing transverse momentum $\vec{p}_T^{\text{miss}}$, is known. A generalization of the transverse mass, the M_{T2} variable, is defined as:

$$M_{T2}(m_X) = \min_{\vec{p}_T^{X(1)} + \vec{p}_T^{X(2)} = \vec{p}_T^{\text{miss}}} \left[\max\left(M_T^{(1)}, M_T^{(2)}\right)\right], \qquad (2.2)$$

where the unknown mass m_X is a free parameter. The minimization is performed over trial momenta of the undetected particles fulfilling the $\vec{p}_T^{\text{miss}}$ constraint.

In this analysis, all visible objects, such as jets, are clustered into two pseudojets. For this purpose, we use the hemisphere algorithm defined in section 13.4 of ref. [20]. The algorithm is seeded by the two jets with largest dijet invariant mass. The clustering is performed by minimizing the Lund distance measure [21, 22]. Standard model multijet events, interpreted as two pseudojets, may give rise to large M_{T2} if both pseudojets have large masses. Setting $m^{\text{vis}(i)} = 0$ in eq. (2.1) suppresses the multijet contributions without affecting signal sensitivity, since the kinematic terms of eq. (2.1) are large for most new-physics scenarios. In the following, M_{T2} is computed using $E_T^{\text{vis}(i)}$, $\vec{p}_T^{\text{vis}(i)}$ ($i = 1, 2$), and $\vec{p}_T^{\text{miss}}$, setting both $m^{\text{vis}(i)}$ terms in eq. (2.1) to zero.

Although most the background from SM multijet events is thus characterized by small values of M_{T2}, a residual background at large M_{T2} arises from multijet events in which the two pseudojets are not back-to-back because of jet energy mismeasurements. Further selection criteria are applied to suppress these events, as discussed in section 4.

3   Detector and trigger

The central feature of the CMS apparatus is a superconducting solenoid of 6 m internal diameter, providing a magnetic field of 3.8 T. Within the superconducting solenoid volume are a silicon pixel and strip tracker, a lead-tungstate crystal electromagnetic calorimeter, and a brass/scintillator hadron calorimeter, each composed of a barrel and two endcap sections. Muons are measured in gas-ionization detectors embedded in the steel flux-return yoke outside the solenoid. Extensive forward calorimetry complements the coverage provided by the barrel and endcap detectors. The detector is nearly hermetic, covering

$0 < \phi < 2\pi$ in azimuth, and thus allows the measurement of momentum balance in the plane transverse to the beam direction. The first level of the CMS trigger system, composed of custom hardware processors, uses information from the calorimeters and muon detectors to select the most interesting events in a fixed time interval of less than $4\,\mu s$. The high level trigger processor farm further decreases the event rate, from around $100\,\mathrm{kHz}$ to around $300\,\mathrm{Hz}$, before data storage. A more detailed description of the CMS detector, together with a definition of the coordinate system used and the relevant kinematic variables, can be found in ref. [23].

Events are selected using three complementary triggers. A trigger based on the scalar sum of jet p_T values (H_T) requires $H_\mathrm{T} > 650\,\mathrm{GeV}$. A second trigger requires $E_\mathrm{T}^\mathrm{miss} > 150\,\mathrm{GeV}$, where $E_\mathrm{T}^\mathrm{miss}$ is the magnitude of $\vec{p}_\mathrm{T}^{\,\mathrm{miss}}$. A third trigger requires $H_\mathrm{T} > 350\,\mathrm{GeV}$ and $E_\mathrm{T}^\mathrm{miss} > 100\,\mathrm{GeV}$. The trigger efficiency is measured to be larger than 99% for events that satisfy the event selection criteria outlined in section 4.

4 Data sets and event selection

The event selection is designed using simulated samples of background and signal processes. Background events are generated with the MADGRAPH 5 [24], PYTHIA 6.4.26 [22], and POWHEG 1.0 [25] programs. Signal event samples based on simplified model scenarios (SMS) [26] are generated using the MADGRAPH 5 program, with the decay branching fractions of SUSY particles set either to 0% or 100% depending on the SUSY scenario under consideration. We also generate signal events in the context of the constrained minimal supersymmetric SM (cMSSM/mSUGRA) [27]. The cMSSM/mSUGRA events are generated using the PYTHIA program, with the SDECAY [28] program used to describe the SUSY particle decay branching fractions and the SOFTSUSY [29] program to calculate the SUSY particle mass spectrum. The PYTHIA program is used to describe the parton shower and hadronization. While all generated background samples are processed with the detailed simulation of the CMS detector response, based on GEANT 4 [30], for signal samples the detector simulation is performed using the CMS fast simulation package [31]. Detailed cross checks are conducted to ensure that the results obtained with fast simulation are in agreement with the ones obtained with GEANT-based detector simulation. For SM backgrounds, the most accurate calculations of the cross sections available in the literature are used [32, 33]. These are usually at next-to-leading order (NLO) in α_S. For the SUSY signal samples, cross sections are calculated at NLO [34–38] using the PROSPINO 2.1 [39] program.

The data and simulated events are reconstructed and analyzed in an identical manner. The event reconstruction is based on the particle-flow (PF) algorithm [40, 41], which reconstructs and identifies charged hadrons, neutral hadrons, photons, muons, and electrons. Electrons and muons are required to have transverse momentum $p_\mathrm{T} > 10\,\mathrm{GeV}$ and pseudorapidity $|\eta| < 2.4$. For electrons, the transition region between barrel and endcaps $(1.442 < |\eta| < 1.566)$ is excluded because the electron reconstruction in this region is not optimal. An isolation requirement is also employed, requiring that the p_T sum of photons, charged hadrons, and neutral hadrons, in a cone of $\Delta R = \sqrt{(\Delta\eta)^2 + (\Delta\phi)^2} = 0.3$ along the lepton direction, divided by the lepton p_T value, be less than 0.15 for electrons and

0.20 for muons. The isolation value is corrected for the effects of pileup, that is, multiple pp collisions within the same bunch crossing as the primary interaction. The electron and muon reconstruction and identification criteria are described in refs. [42] and [43], respectively. All particles, except the isolated electrons and muons, are clustered into PF jets [44] using the anti-k_T jet-clustering algorithm [45] with a size parameter of 0.5. The jet energy is calibrated by applying correction factors as a function of the p_T and the η of the jet [44]. The effect of pileup on jet energies is treated as follows: tracks not associated with the primary interaction are removed from the jet; for the neutral part of the jet, the effect of pileup is reduced using the FASTJET pileup subtraction procedure [46, 47]. All jets are required to satisfy basic quality criteria (jet ID [48]), which eliminate, for example, spurious events due to calorimeter noise. Jets are also required to have $p_T > 20\,\text{GeV}$ and $|\eta| < 2.4$. Jets are b-tagged using the medium working point of the combined secondary vertex (CSV) algorithm [49]. Tau leptons are reconstructed in their decays to one or three charged particles [50] and are required to have $p_T > 20\,\text{GeV}$ and $|\eta| < 2.3$. The τ leptons are also required to satisfy a loose isolation selection: the p_T-sum of charged hadrons and photons that appear within $\Delta R < 0.5$ of the candidate τ-lepton direction is required to be less than $2\,\text{GeV}$ after subtraction of the pileup contribution. Throughout this paper, any mention of a τ lepton refers to its reconstructed hadronic decay. Photons [51] are required to have $p_T > 20\,\text{GeV}$, $|\eta| < 2.4$, and to not appear in the transition region between the barrel and endcap detectors. Photons are further required to satisfy selection criteria based on the shape of their calorimetric shower, to deposit little energy in the hadron calorimeter, and to fulfill isolation requirements.

The missing transverse momentum vector $\vec{p}_T^{\text{miss}}$ is defined as the projection onto the plane perpendicular to the beam axis of the negative vector sum of the momenta of all reconstructed particles in the event. Its magnitude is referred to as E_T^{miss}. The hadronic activity in the event, H_T, is defined to be the scalar p_T sum of all accepted jets with $p_T > 50\,\text{GeV}$ and $|\eta| < 3.0$. Events selected with the pure-H_T trigger described in section 3 are required to satisfy $H_T > 750\,\text{GeV}$. Events selected with one of the two other triggers are required to satisfy $H_T > 450\,\text{GeV}$ and $E_T^{\text{miss}} > 200\,\text{GeV}$.

Corrections for differences observed between the simulation and data due to the jet energy scale [44], the b-tagging efficiencies [49], and the p_T spectrum of the system recoil [52] are applied to simulated events.

Events are required to contain at least two jets that, in addition to the previous general jet requirements, have $p_T > 100\,\text{GeV}$. To reduce the background from events with W($\ell\nu$)+jets and top-quark production, events are rejected if they contain an isolated electron, muon, or τ lepton. Background from multijet events, which mostly arises because of jet energy misreconstruction, is reduced by requiring the minimum difference $\Delta\phi_{\text{min}}$ in azimuthal angle between the $\vec{p}_T^{\text{miss}}$ vector and one of the four jets with highest p_T to exceed 0.3 radians. To reject events in which E_T^{miss} arises from unclustered energy or from jets aligned near the beam axis, a maximum difference of $70\,\text{GeV}$ is imposed on the magnitude of the vectorial difference between $\vec{p}_T^{\text{miss}}$ and the negative vector sum of the p_T of all leptons and jets. Finally, events with possible contributions from beam halo processes or anomalous noise in the calorimeter or tracking systems are rejected [53].
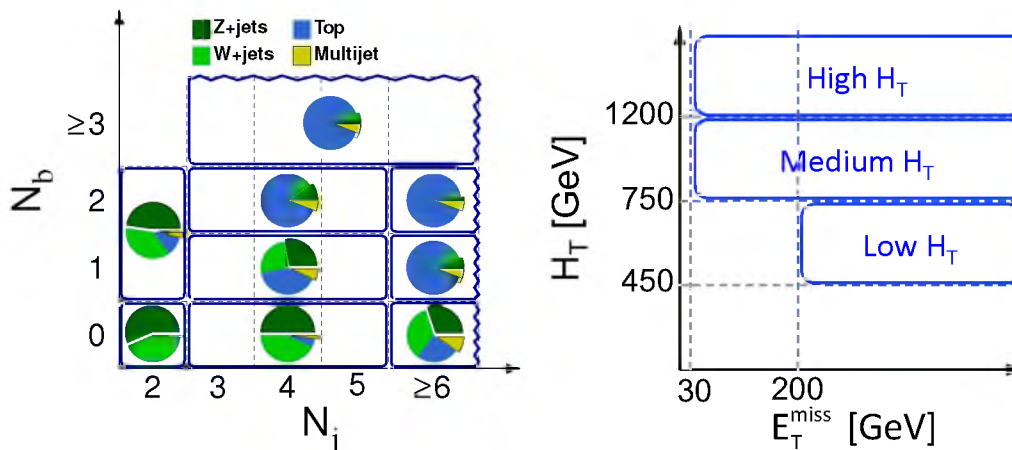
Figure 1. Definition of the topological signal regions in terms of the number of jets N_j and the number of b-tagged jets N_b (left), and their subsequent division in terms of H_T and E_T^{miss} (right). The pie charts illustrate the expected contributions from different SM processes in the different signal regions; they are similar in all three H_T regions.

5 Search strategy

The M_{T2}-based search strategy is outlined in this section. For both the inclusive-M_{T2} and the M_{T2}-Higgs searches, all selected jets are clustered into two pseudojets as described in section 2. Several mutually exclusive signal regions are defined to optimize the search for a wide variety of new-physics models. The definition of signal regions is based on the event topology and event kinematic variables. The more general inclusive-M_{T2} search is described first.

The inclusive-M_{T2} and M_{T2}-Higgs searches are not mutually exclusive. All but 4% of the events selected by the M_{T2}-Higgs search are also selected by the inclusive-M_{T2} search.

5.1 Inclusive-M_{T2} search

For the inclusive-M_{T2} search, nine regions, called topological regions, are defined by N_j and N_b, the numbers of jets and b-tagged jets in the event with $p_T > 40\,\mathrm{GeV}$, as illustrated in figure 1 (left). These regions are chosen after testing the sensitivity of the search to various SUSY SMS models using simulated data. The regions with $N_b = 0$ are the most sensitive to the production of gluinos that do not decay to top and bottom quarks, and to the production of squarks of the first two generations. The regions with $N_b > 0$ and low (high) values of N_j are designed for bottom- and top-squark production with decays to bottom (top) quarks. Finally, the signal regions with $N_j \geq 3$ and $N_b \geq 3$ provide extra sensitivity to final states with multiple bottom or top quarks, for example from gluino pair-production. Since the values of M_{T2} and H_T in a SUSY event depend strongly on the mass of the initially produced SUSY particles, a wide range of values in M_{T2} and H_T is considered. Each of the nine topological regions is divided into three sub-regions of H_T, as shown in figure 1 (right): the low-H_T region $450 < H_T \leq 750\,\mathrm{GeV}$, the medium-$H_T$ region $750 < H_T \leq 1200\,\mathrm{GeV}$, and the high-$H_T$ region $H_T > 1200\,\mathrm{GeV}$.

	Low-H_T region M_T2 bin [GeV]			Medium-H_T region M_T2 bin [GeV]			High-H_T region M_T2 bin [GeV]	
$N_\mathrm{j}=2$, $N_\mathrm{b}=0$	200–240	350–420	570–650	125–150	220–270	425–580	120–150	260–350
	240–290	420–490	>650	150–180	270–325	580–780	150–200	350–550
	290–350	490–570		180–220	325–425	>780	200–260	>550
$N_\mathrm{j}=2$, $N_\mathrm{b}\geq1$	200–250	310–380	450–550	100–135	170–260	>450	100–180	
	250–310	380–450	>550	135–170	260–450		>180	
$N_\mathrm{j}=3$–5, $N_\mathrm{b}=0$	200–240	420–490		160–185	300–370	>800	160–185	350–450
	240–290	490–570		185–215	370–480		185–220	450–650
	290–350	570–650		215–250	480–640		220–270	>650
	350–420	>650		250–300	640–800		270–350	
$N_\mathrm{j}=3$–5, $N_\mathrm{b}=1$	200–250	310–380	460–550	150–175	210–270	380–600	150–180	230–350
	250–310	380–460	>550	175–210	270–380	>600	180–230	>350
$N_\mathrm{j}=3$–5, $N_\mathrm{b}=2$	200–250	325–425		130–160	200–270	>370	130–200	
	250–325	>425		160–200	270–370		>200	
$N_\mathrm{j}\geq6$, $N_\mathrm{b}=0$	200–280	>380		160–200	250–325	>425	160–200	>300
	280–380			200–250	325–425		200–300	
$N_\mathrm{j}\geq6$, $N_\mathrm{b}=1$	200–250	>325		150–190	250–350		150–200	>300
	250–325			190–250	>350		200–300	
$N_\mathrm{j}\geq6$, $N_\mathrm{b}=2$	200–250	>300		130–170	220–300		130–200	
	250–300			170–220	>300		>200	
$N_\mathrm{j}\geq3$, $N_\mathrm{b}\geq3$	200–280	>280		125–175	175–275	>275	>125	

Table 1. Definition of the signal regions used in the inclusive-M_T2 search.

Each of these regions is examined in bins of M_T2, where the number of bins (up to nine) depends on the specific topological and H_T selection. By design, the lowest bin in M_T2 is chosen such that the multijet background is expected to be less than $\sim$1–10% of the total background. The minimum threshold on M_T2 varies between 100 and 200 GeV, depending on the topological region and the H_T requirement. The edges of the M_T2 bins are adjusted to ensure that there are a sufficient number of events in each bin of the corresponding control samples for the background evaluation (section 6). The definitions of all signal regions are specified in table 1.

Figure 2 shows the M_T2 distributions in simulation and data for the low-, medium-, and high-H_T selections, inclusively in all signal regions of the N_j–N_b plane. For $M_\mathrm{T2}<80$ GeV the distribution in the medium- and high-H_T regions is completely dominated by multijet events. For this reason, these bins are used only as control regions.

In the signal regions with $N_\mathrm{j}=2$ or $N_\mathrm{b}=0$, the dominant background is from Z ($\nu\overline{\nu}$)+jets production. The next-most important background is from W($\ell\nu$)+jets events, while the background from t$\overline{\mathrm{t}}$ +jets events is small. In the regions with $N_\mathrm{b}=1$ all three processes (Z ($\nu\overline{\nu}$)+jets, W($\ell\nu$)+jets, and t$\overline{\mathrm{t}}$ +jets production) are important. For all regions requiring multiple b-tagged jets, t$\overline{\mathrm{t}}$ +jets events are the dominant source of background. The t$\overline{\mathrm{t}}$ +jets contribution to the total background typically increases with the jet multiplicity and is important for all selections with $N_\mathrm{j}\geq6$, regardless of the N_b selection. The
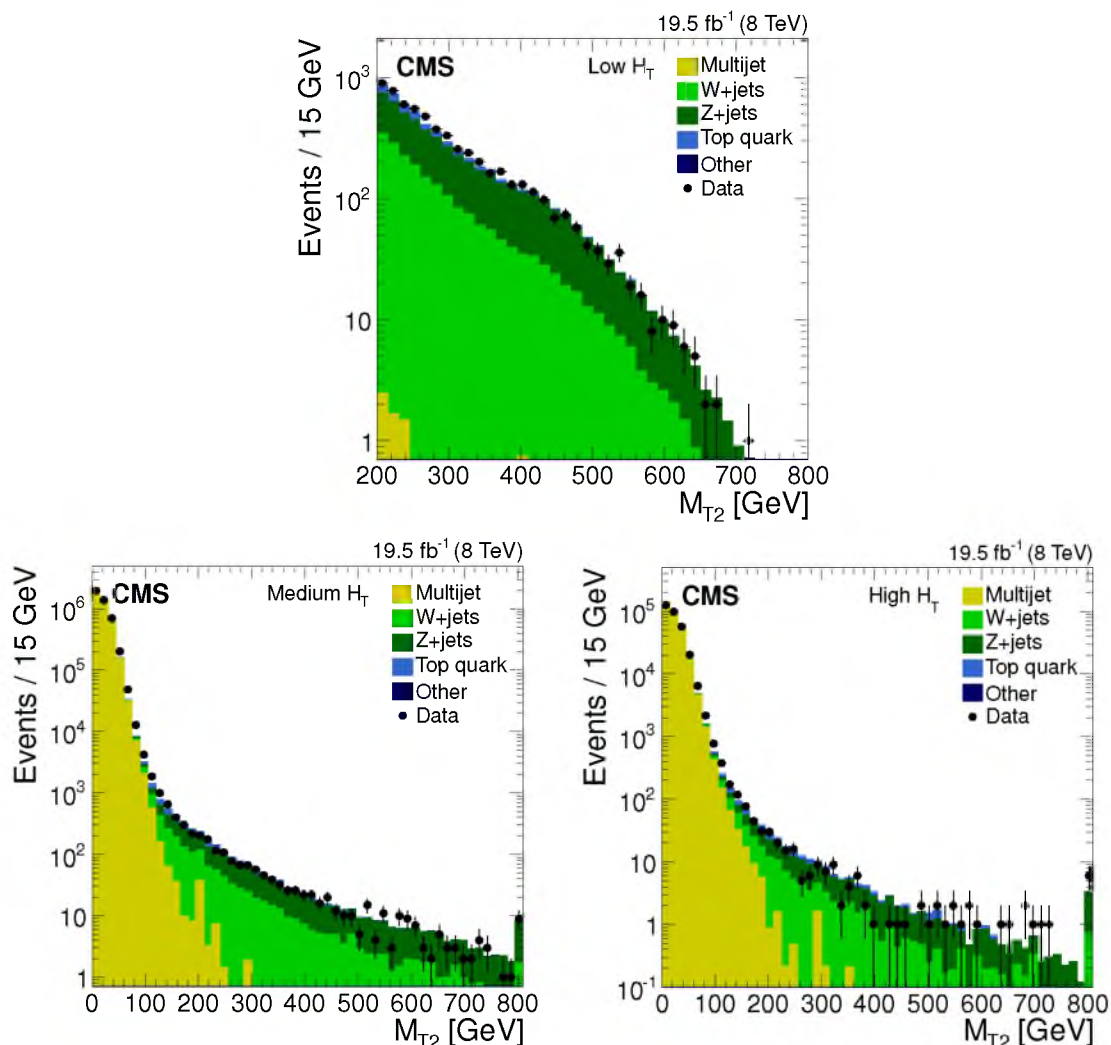
Figure 2. Distribution of the M_{T2} variable after the low-H_T (top), medium-H_T (bottom left), and high-H_T (bottom right) event selections, respectively. The event yields are integrated in the (N_j, N_b) plane over all the topological signal regions, for both simulated and data samples. These plots serve as an illustration of the background composition of the M_{T2} distributions.

relative contribution of $t\bar{t}$ +jets production decreases with increasing M_{T2} because of the natural cutoff of M_{T2} above the top-quark mass for these events.

Contributions from other backgrounds, such as γ+jets, Z ($\ell^+\ell^-$)+jets, and diboson production, are found to be negligible.

5.2 M_{T2}-Higgs search

The M_{T2}-Higgs search is designed to select events with a light h boson produced in a cascade of supersymmetric particles initiated through the strong pair production of squarks or gluinos. As the dominant decay mode of the h boson in many SUSY models is h → $b\bar{b}$, a signature of a SUSY signal would be an excess in the invariant mass distribution of the selected b-tagged jet pairs, M_{bb}. An excess could help identify a preferred new-

physics model, as the associated new particles would couple to the Higgs sector. Such an identification is not possible with the inclusive-M_{T2} search.

Within a cascade of SUSY particles, the h boson is produced together with the LSP in the decays of neutralinos, such as $\widetilde{\chi}_2^0 \rightarrow \widetilde{\chi}_1^0 + h$. As the neutralino $\widetilde{\chi}_2^0$ can be a typical decay product of squarks and gluinos, the cross section for this kind of processes is among the largest in a large part of the SUSY parameter space. The final state contains at least two b-tagged jets, multiple hard jets, and a large value of M_{T2}.

For the M_{T2}-Higgs search, b-tagged jets are required to have $p_T > 20\,\text{GeV}$. The event selection requires at least two b-tagged jets, along with $N_j \geq 4$. The two b-tagged jets stemming from the h boson decay are generally expected to appear within the same pseudojet, as they originate from the same decay chain. Using b-tagged jets within the same pseudojet, a b-tagged jet pair is selected if it has $\Delta R(b_1, b_2) < 1.5$. If multiple pairs are found in one or both pseudojets, the pair with the smallest $\Delta R(b_1, b_2)$ is chosen. If no pair is found within the same pseudojet, pairs with b-tagged jets in different pseudojets are considered. If none of the pairs has $\Delta R(b_1, b_2) < 1.5$, the event is rejected. For signal events containing b quarks from the h boson decay, the efficiency to find the correct pair of b-tagged jets is about 70%.

Using the known h boson mass of 125 GeV [54, 55], 12 signal regions are defined as 15 GeV-wide bins in the $20 < M_{bb} < 200\,\text{GeV}$ range. Each of these signal regions is further divided into two sub-regions as follows: a low-H_T selection requiring $450 < H_T \leq 750\,\text{GeV}$, $E_T^{\text{miss}} > 200\,\text{GeV}$, and $M_{T2} > 200\,\text{GeV}$; and a high-H_T selection requiring $H_T > 750\,\text{GeV}$ and $M_{T2} > 125\,\text{GeV}$.

The overall yields of the main SM backgrounds ($t\bar{t}$ +jets, W($\ell\nu$)+jets, and Z ($\nu\overline{\nu}$)+jets) are estimated using the same methods as for the inclusive-M_{T2} analysis. The contribution of the SM production of the Higgs boson is negligible in the search regions of this analysis. The shapes of the M_{bb} distributions for signal and the various backgrounds are obtained from simulation. Since in simulation we observe no appreciable correlation between M_{T2} and M_{bb} in either the signal or background sample, the shape of the M_{bb} distribution is obtained from large simulated samples with relaxed M_{T2} requirements. An uncertainty due to the looser M_{T2} selection is taken into account. Further uncertainties in the shapes are assessed by varying several modelling parameters of the simulation.

6 Background estimation

This section describes the procedures used to estimate the main backgrounds: multijet events, Z+jets events where the Z boson decays to neutrinos, and W+jets and $t\bar{t}$ +jets events where one W boson decays leptonically but the corresponding charged lepton lies outside the acceptance of the analysis, is not reconstructed, or is not isolated. The same background estimation procedures are used for both the inclusive-M_{T2} and M_{T2}-Higgs searches.

6.1 Determination of the multijet background

The multijet background consists of direct multijet production, but also of events with $t\bar{t}$ pairs or vector bosons that decay hadronically. From figure 2, the multijet background

is expected to be negligible at large values of M_{T2}. This background, arising from difficult-to-model jet energy mismeasurements, is nonetheless subject to considerable uncertainty. A method based on data control samples is used to predict this background. The method relies on M_{T2} and the variable $\Delta\phi_{\text{min}}$, described in section 4. In general terms, the multijet background entering each of the signal regions, for which a selection requirement is $\Delta\phi_{\text{min}} > 0.3$, is estimated from a corresponding control region defined by the same criteria as the signal regions except for $\Delta\phi_{\text{min}}$, which is required to be less than 0.2. The control regions are dominated by multijet event production.

The transfer factor between control and signal regions, and our parameterization thereof, are given by

$$r(M_{\text{T2}}) \equiv \frac{N(\Delta\phi_{\text{min}} > 0.3)}{N(\Delta\phi_{\text{min}} < 0.2)} = \exp(a - b\, M_{\text{T2}}) + c \qquad \text{for } M_{\text{T2}} > 50\,\text{GeV}. \tag{6.1}$$

The parameters a and b are obtained from a fit to data in the region $50 < M_{\text{T2}} < 80\,\text{GeV}$, where the contributions of electroweak and top-quark (mainly $t\bar{t}$ +jets events) production are small. The constant term c is only measurable in control samples requiring high-M_{T2} values. For these events, however, the non-multijet contribution is dominant, and so c cannot be obtained from a fit to data. Therefore, the parameterization of $r(M_{\text{T2}})$ is fixed to a constant for $M_{\text{T2}} > 200\,\text{GeV}$. This constant is chosen as the value of the exponential fit to $r(M_{\text{T2}})$ at $M_{\text{T2}} = 200\,\text{GeV}$.

The parameterization is validated by fitting $r(M_{\text{T2}})$ to a sample of simulated multijet events, and multiplying this ratio by the number of events found in data with $\Delta\phi_{\text{min}} < 0.2$. The result is compared to the number of events in data with $\Delta\phi_{\text{min}} > 0.3$, after subtraction of the non-multijet contribution using simulation. An example is shown in figure 3. The prediction is seen to provide a conservative estimate of the expected multijet background. The robustness of the method is further validated by varying the range of M_{T2} in which the exponential term is fitted, and by changing the $\Delta\phi_{\text{min}}$ requirement used to define the control regions.

In the low-H_{T} regions, the $E_{\text{T}}^{\text{miss}}$ requirement of the triggers distorts $r(M_{\text{T2}})$ for low values of M_{T2}. Therefore, the data selected by the standard triggers cannot be used to obtain $r(M_{\text{T2}})$. Other triggers, based on H_{T} only, are used instead. These triggers accept only a small fraction of the events that satisfy the trigger criteria ("prescaled"), allowing access to the low-H_{T} region without a $E_{\text{T}}^{\text{miss}}$ requirement.

The dominant sources of uncertainty for this method include the statistical uncertainty of the fit, the stability of the fit under variations of the fit conditions, the statistical uncertainty of the control region with $\Delta\phi_{\text{min}} < 0.2$ used for the extrapolation, and a 50% uncertainty assigned to the choice of the M_{T2} value used to define the constant term in the functional form of $r(M_{\text{T2}})$. In signal regions with low M_{T2}, where the exponential term of eq. (6.1) dominates the constant term, this method provides a relatively accurate estimate of the background, with uncertainties as small as 10% that increase to around 50% for signal regions with less statistical precision. For signal regions with large M_{T2}, the constant term dominates and the uncertainty increases to 50–100%. Note that at large M_{T2}, the estimate of the multijet background provided by this method, while conservative, is nonetheless negligible compared to the contributions of the other backgrounds.
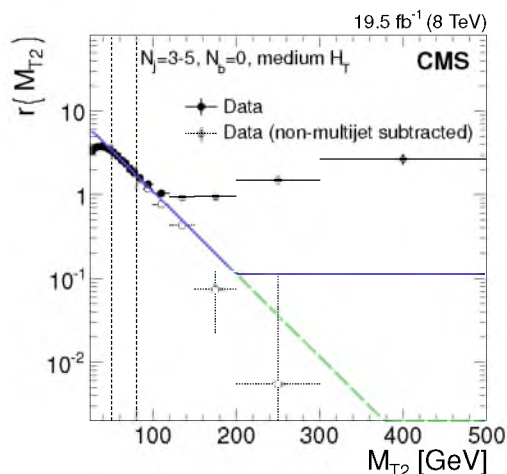
Figure 3. The ratio $r(M_{T2})$, described in the text, as a function of M_{T2} for events satisfying the medium-H_T and the ($N_j = 3$–$5, N_b = 0$) requirements of the inclusive-M_{T2} search. The solid circle points correspond to simple data yields, while the points with open circles correspond to data after the subtraction of the non-multijet backgrounds, as estimated from simulation. Two different functions, whose exponential components are fitted to the data in the region $50 < M_{T2} < 80 \, \text{GeV}$, are shown. The green dashed line presents an exponential function, while the blue solid line is the parameterization used in the estimation method.

6.2 Determination of the W($\ell\nu$)+jets and leptonic top-quark background

The background from W($\ell\nu$)+jets and top-quark production (mainly $t\bar{t}$ +jets events, but also single top-quark production) stems from events with a leptonically decaying W boson in which the charged lepton either lies outside the detector acceptance, or lies within the acceptance but fails to satisfy the lepton reconstruction, identification, or isolation criteria. Since these events arise from a lepton (e, μ, or τ lepton) that is not found, we call them "lost-lepton" events. For both sources of lost leptons, the contribution from τ leptons is slightly higher than from electrons or muons since the reconstruction efficiency for τ leptons is smaller and the acceptance criteria are more stringent than for the other two types of leptons. According to simulation, around 40% of this background can be attributed to events containing a lost τ lepton. The contribution of electron and muon events is of equal size.

For each signal region, the lost-lepton background is estimated in a corresponding data control sample for which the full event selection is applied, with the exception of the lepton veto, i.e. exactly one charged lepton (e, μ, or τ lepton) is required instead of zero. To reduce the potential contribution of signal events to the control samples, the transverse mass of the lepton-E_T^{miss} system is required to satisfy $M_T < 100 \, \text{GeV}$. The M_{T2} distributions of events satisfying the selection as outlined in section 4, but after requiring one reconstructed and identified lepton, are shown in figure 4 for both data and simulation.

After subtracting the number of events expected due to the misidentification of hadrons as leptons and due to leptons from hadron decays, the numbers of events in the one-lepton control samples are scaled by a lost-lepton factor $R_{\ell\ell} = [1 - \varepsilon(\ell)]/[\varepsilon(\ell)\varepsilon(M_T)]$, where $\varepsilon(\ell)$
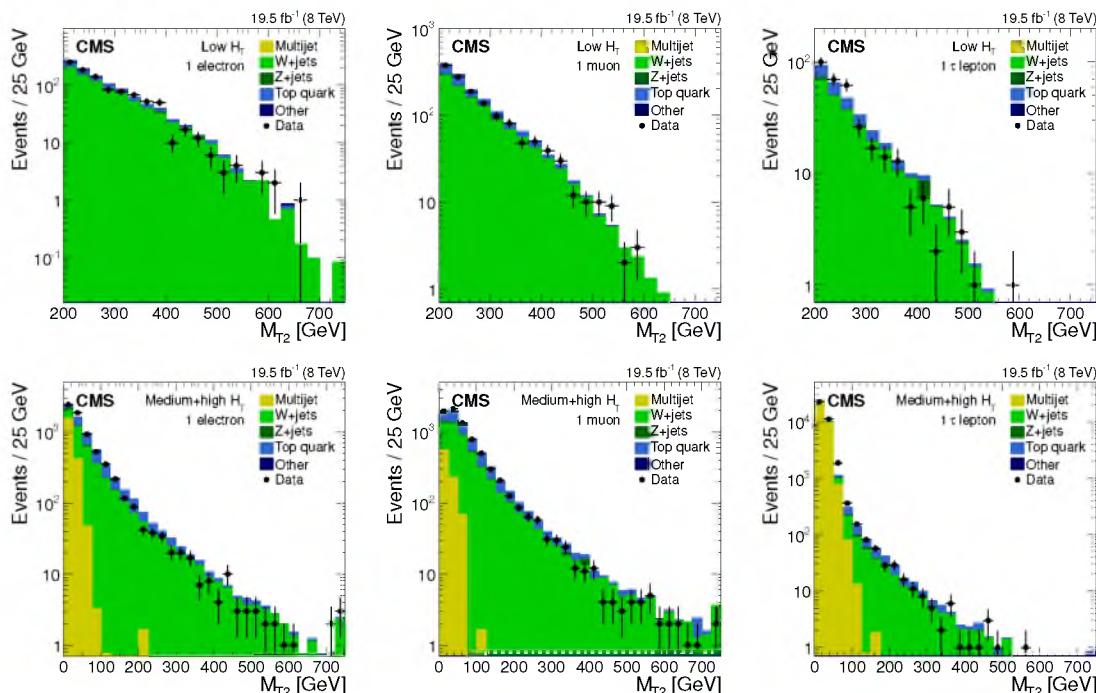
Figure 4. Distribution of the M_{T2} variable for events with one electron (left), one muon (middle), or one τ lepton (right) in data and simulation. The events satisfy either the low-H_T selection (top) or either of the medium- and high-H_T selections (bottom). They also satisfy the remaining inclusive-M_{T2} selection requirements, with the exception of the lepton veto. Finally, the condition $M_T < 100\,\text{GeV}$ is imposed on the charged lepton-E_T^{miss} system.

is the combined lepton efficiency and acceptance, and $\varepsilon(M_T)$ is the efficiency of the M_T selection. This factor $R_{\ell\ell}$ is therefore the transfer factor from the control region to the signal region, obtained in simulation.

For large values of M_{T2}, we expect very few events with a single reconstructed charged lepton. Therefore, the estimation of the lost-lepton background is performed in data for all topological regions in (N_j, N_b) and for the different H_T selections, but integrating over all M_{T2} bins. The factor $R_{\ell\ell}$ is recalculated for each topological signal region and for the different selections in H_T. The estimated number of background events is divided among the different M_{T2} bins using the shape of the M_{T2} distribution as predicted by simulation.

The systematic uncertainty in the integrated lost-lepton background estimate includes the uncertainties in the lepton efficiencies, acceptance, and the subtraction of the lepton events associated with misidentification and hadron decays. These uncertainties are obtained by studying the differences between data and simulation using so-called tag-and-probe [56] and tight-to-loose [57] methods. These uncertainties amount to about 10–20%. Including the statistical uncertainties from the data control regions, the total uncertainty of the lost-lepton background ranges from 10 to 65%. The uncertainty in the shape of the M_{T2} distribution is estimated by varying parameters in the simulation. The most important of these uncertainties are the recoil modelling [52] (20%), the matching scale, the renormalization and factorization scales (10–20%), and the jet energy scale [44] (10%). The

numbers in parentheses correspond to maximal variations in the M_{T2} shape, but the overall normalization is not affected since it is predicted using the aforementioned method. The differences in shape between the distributions in data and simulation, shown in figure 4, lie within these uncertainties.

The effect of signal contributions to the lost-lepton control samples can be significant and is taken into account before the interpretations presented in sections 9 and 10 are performed. Specifically, the predicted yield in the signal regions is corrected by subtracting the additional signal contribution caused by the possible presence of the signal in the lost-lepton control sample.

6.3   Determination of the $Z(\nu\bar{\nu})$+jets background

The Z $(\nu\bar{\nu})$+jets background is estimated by selecting a control sample of γ+jets events and then subtracting the photon momentum in the computation of all the relevant event quantities, such as M_{T2}, in order to replicate the decay of a Z boson into undetected neutrinos. After the subtraction of the photon momentum, the $\vec{p}_{\mathrm{T}}^{\mathrm{miss}}$ and the M_{T2} variables are recalculated and the event selections corresponding to the different signal regions are applied. The number of selected events, which is rescaled as described below, provides the background estimate for the Z $(\nu\bar{\nu})$+jets process.

As discussed in ref. [58], the Z+jets and γ+jets processes differ because of the different electroweak couplings and the non-zero Z-boson mass m_{Z}. For vector boson $p_{\mathrm{T}} \gg m_{\mathrm{Z}}$, however, the ratio of cross sections for prompt-photon to Z-boson production is determined by the ratio of the couplings of the respective boson to quarks, and thus approaches a constant value. In this range of the boson p_{T}, the distributions of H_{T} and other kinematic observables are very similar for the Z+jets and γ+jets processes. The γ+jets process, with its relatively large event yield, is thus well suited to provide an estimate of the Z $(\nu\bar{\nu})$+jets background.

Figure 5 shows a comparison between data and simulation for the M_{T2} distribution in γ+jets control samples, for which N_{b} =0 is required. The photon $\vec{p}_{\mathrm{T}}$ is added to $\vec{p}_{\mathrm{T}}^{\mathrm{miss}}$ vector and all event variables are recalculated. To reduce the potential contribution of signal events to these control samples, we require the reconstructed $E_{\mathrm{T}}^{\mathrm{miss}}$ to be less than $100\,\mathrm{GeV}$ prior to including the reconstructed photon momentum. For the low-H_{T} signal regions, the γ+jets events are selected with a single-photon trigger, which requires the photon p_{T} to exceed $150\,\mathrm{GeV}$. The single-photon trigger is used because the triggers discussed in section 3 are unable to select events with low enough $E_{\mathrm{T}}^{\mathrm{miss}}$. For the medium- and high-H_{T} signal regions, the triggers discussed in section 3 are used.

The selected photon control samples contain both genuine prompt-photon events and events with collinear pairs of photons that stem from neutral-meson decays within jets and are reconstructed as single photons. The prompt-photon fraction in the control samples is obtained by means of a maximum likelihood fit of templates from simulation to a photon shower shape variable in data. The shower shape variable that we use is $\sigma_{\eta\eta}$, which is a measure of the lateral extent in η of the photon energy cluster in the calorimeter [51]. The fit is performed separately in the electromagnetic calorimeter barrel and endcap detectors, for events with $N_{\mathrm{b}} = 0$ and with no requirement on M_{T2}. This sample of events is dominated by
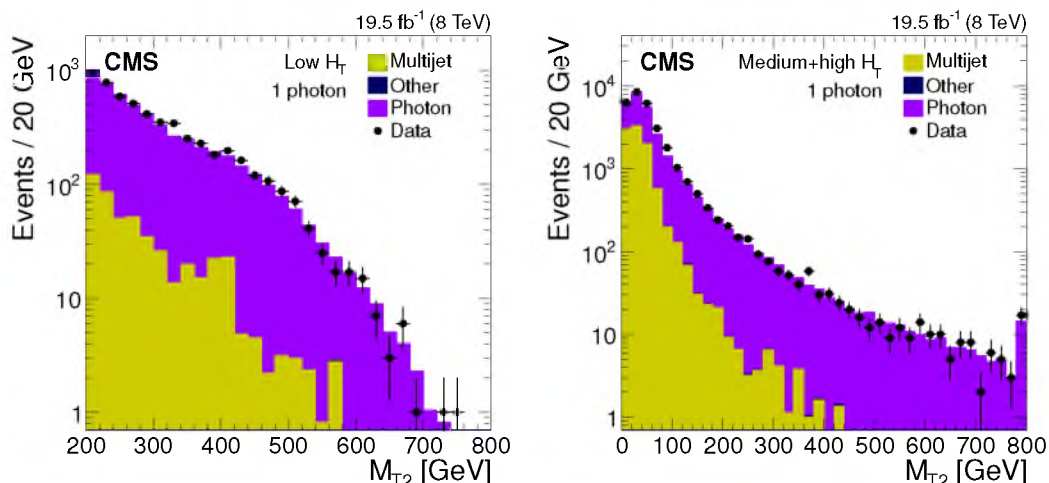
Figure 5. Distribution of the M_{T2} variable for data and simulation after requiring the presence of one photon, $N_b = 0$, and the remainder of the inclusive-M_{T2} selection criteria. Events satisfying the low-H_T selection (left), and the medium- and high-H_T selections (right) are shown. For these results, M_{T2} is calculated after adding the photon p_T to the E_T^{miss} vector.

low-p_T photons, for which the shower shape variable provides high discrimination between prompt photons and photons from neutral-meson decays. Starting from the overall prompt-photon fraction observed in data, we use simulation to extrapolate the contributions of the two types of photon events in M_{T2}. For each signal region with $N_b = 0$, the final Z ($\nu\overline{\nu}$)+jets background estimate is obtained from the number of prompt-photon events, rescaled by the M_{T2}-dependent ratio of Z ($\nu\overline{\nu}$)+jets to γ+jets events from simulation. The $Z(\nu\overline{\nu})/\gamma$ ratio increases as a function of the photon p_T and reaches a constant value above 350 GeV, as shown in figure 6.

The accuracy of the Z-boson p_T distribution in simulation is validated using a control sample of dileptonic Z-boson events, i.e. $Z \rightarrow e^+e^-$ or $\mu^+\mu^-$, selected with dilepton triggers. Here, analogously to the photon control sample, the dilepton momentum is subtracted in the computation of all relevant event quantities, such as M_{T2}, in order to model the $Z \rightarrow \nu\overline{\nu}$ decay. From the data-to-simulation comparison of the $Z(\ell^+\ell^-)/\gamma$ ratio as a function of the search variables, a systematic uncertainty of 20% is assigned to the $Z(\nu\overline{\nu})/\gamma$ ratio. For the signal region bins corresponding to $M_{T2} > 350$ GeV, this uncertainty increases to 30% because of large statistical uncertainty in the ratio for events with large M_{T2}. Compared to these uncertainties, the normalization uncertainty associated with the shower shape fit is negligible.

The $Z(\nu\overline{\nu})/\gamma$ ratio may not be well modelled in simulation for $N_b \geq 1$ as the coupling of Z bosons and photons differs for b quarks. If the b-quark content in simulation is mismodelled (for example the modelling of gluon splitting $g \rightarrow b\overline{b}$), the $Z(\nu\overline{\nu})/\gamma$ ratio might be biased in b-quark enriched events. Another biasing effect might be the treatment of the b-quark mass in simulation, which affects the coupling of b quarks to Z bosons and photons. Therefore, the previous procedure is only applied in signal regions with $N_b = 0$. For the $N_b = 1$ case, the results obtained from the $N_b = 0$ control samples are scaled
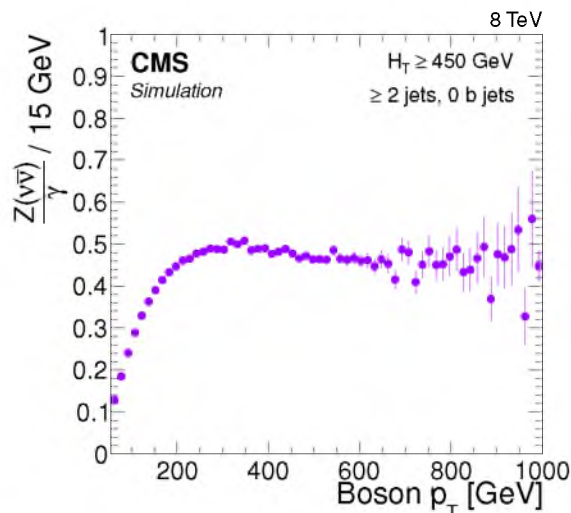
Figure 6. Ratio $Z(\nu\bar{\nu})/\gamma$ of events satisfying the event selection of the $(N_j \geq 2, N_b = 0)$ signal region as a function of the boson p_T. The events are summed inclusively in all H_T sub-regions with $H_T \geq 450 \, \text{GeV}$. The ratio is obtained in simulated events after the photon momentum is included in the E_T^{miss} calculation.

by $Z_{\ell\ell}(1b)/Z_{\ell\ell}(0b)$, the ratio of the numbers of events containing dileptonic decays of the Z boson and $N_b = 1$ or $N_b = 0$, respectively. This ratio is obtained using data from the dilepton control sample for different values of N_j. As the ratio is found to depend neither on M_{T2} nor H_T, its value is measured without any requirement on these two variables, in order to increase the statistical precision of the control samples.

Uncertainties in the $Z_{\ell\ell}(1b)/Z_{\ell\ell}(0b)$ ratio are evaluated by varying the kinematic selections to test the stability of the ratio. The resulting uncertainties are mostly determined by the statistical limitations of the control samples. The size of the uncertainty is 10–30% for the regions with $N_j \leq 5$, while it is 50–75% for regions with $N_j \geq 6$.

For the signal regions with $N_b \geq 2$, the Z $(\nu\bar{\nu})$+jets background is estimated from simulation and is assigned an uncertainty of 100%. We verified that using an uncertainty twice as large, or twice as small, has a negligible impact on the final results. The explanation for this is that for $N_b \geq 2$, the Z $(\nu\bar{\nu})$+jets background is very small compared to the $t\bar{t}$ +jets background.

7 Results

This section reports the number of events observed in the signal regions. The yields are compared with the estimated number of background events as predicted by the methods described in section 6.

7.1 Results for the inclusive-M_{T2} analysis

For the inclusive-M_{T2} search, the final event yields in all signal regions are shown in figures 7–9. The comparison between observed and predicted yields is shown separately for
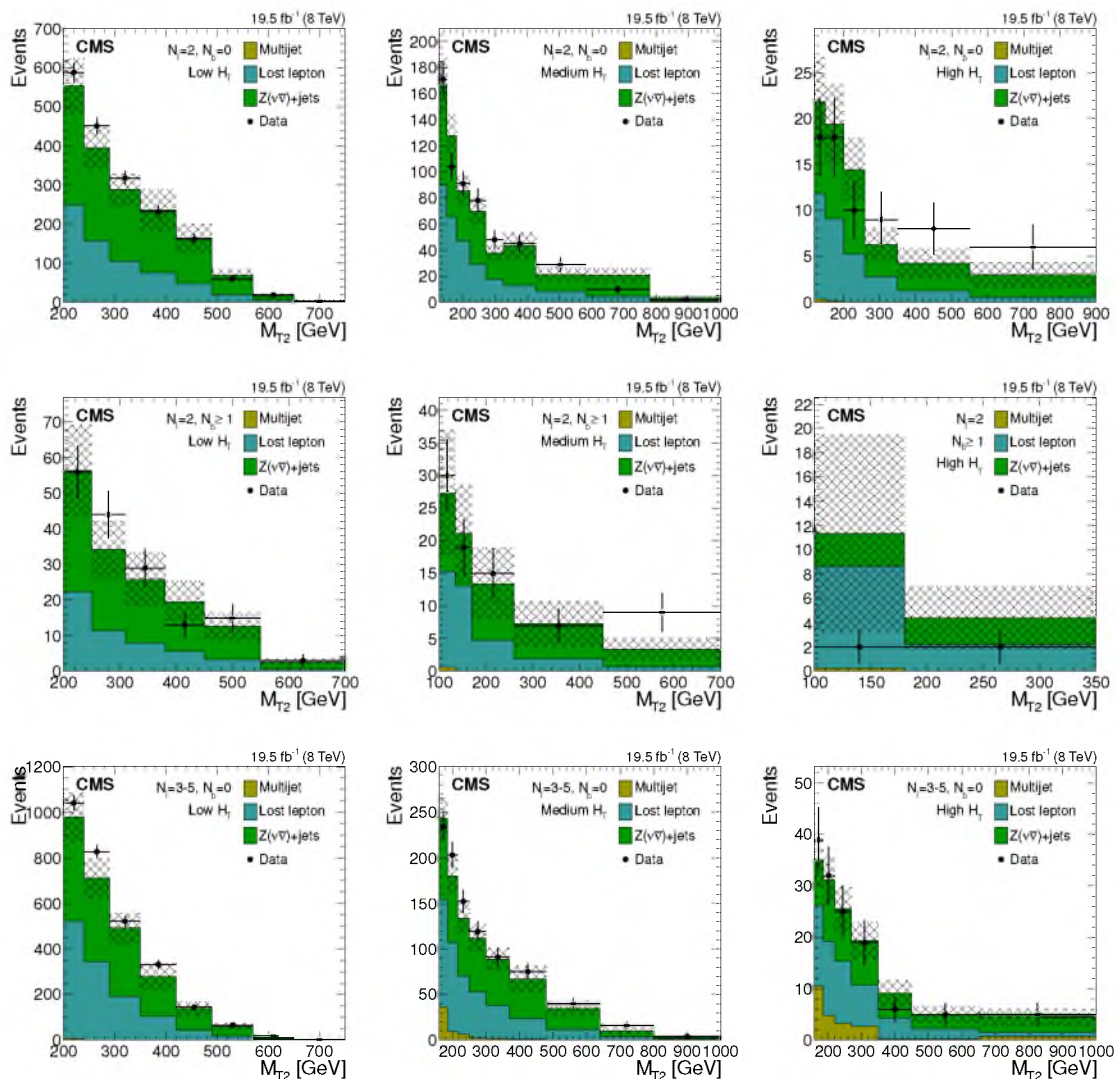
Figure 7. Distributions of the M_{T2} variable for the estimated background processes and for data. Plots are shown for events satisfying the low-H_T (left), the medium-H_T (middle), and the high-H_T (right) selections, and for different topological signal regions (N_j, N_b) of the inclusive-M_{T2} event selection. From top to bottom, these are ($N_j = 2, N_b = 0$), ($N_j = 2, N_b \geq 1$), and ($3 \leq N_j \leq 5, N_b = 0$). The uncertainties in each plot are drawn as the shaded band and do not include the uncertainty in the shape of the lost-lepton background.

different topological regions and for the different H_T selections. The total uncertainty of the background estimates is the quadratic sum of the statistical and systematic uncertainties from the three categories of background. The results are tabulated in table 2. The shape uncertainty in the estimation of the lost-lepton background is not included either for the figures or table.

The level of compatibility between the data and the SM predictions is assessed by computing the pull value for all signal regions, where the pull value is defined for each

Signal region	Low-H_T region			Medium-H_T region			High-H_T region		
	M_{T2} [GeV]	Prediction	Data	M_{T2} [GeV]	Prediction	Data	M_{T2} [GeV]	Prediction	Data
$N_j = 2$, $N_b = 0$	200–240	553±70	588	125–150	167±21	171	120–150	21.9±4.9	18
	240–290	395±53	451	150–180	128±17	104	150–200	19.4±4.3	18
	290–350	288±40	318	180–220	85.8±11.3	91	200–260	14.5±3.4	10
	350–420	236±52	232	220–270	70.0±10.3	78	260–350	6.3±1.8	9
	420–490	165±36	162	270–325	38.1±5.8	48	350–550	4.3±1.6	8
	490–570	68.9±15.5	61	325–425	43.4±10.1	45	>550	3.0±1.4	6
	570–650	17.3±4.3	19	425–580	21.3±4.7	29			
	>650	4.1±1.6	1	580–780	20.8±5.6	10			
				>780	3.5±1.4	2			
$N_j = 2$, $N_b \geq 1$	200–250	56.4±12.8	56	100–135	27.4±9.6	30	100–180	11.4±8.1	2
	250–310	34.2±8.1	44	135–170	21.1±7.5	19	>180	4.4±2.6	2
	310–380	25.9±7.4	29	170–260	13.4±5.4	15			
	380–450	19.9±5.8	13	260–450	7.3±3.5	7			
	450–550	12.6±3.8	15	>450	3.4±1.7	9			
	>550	2.6±0.8	3						
$N_j = 3$–5, $N_b = 0$	200–240	979±108	1041	160–185	243±23	234	160–185	34.9±4.7	39
	240–290	711±86	827	185–215	180±19	203	185–220	31.1±4.7	32
	290–350	492±65	522	215–250	134±16	152	220–270	25.5±4.3	25
	350–420	280±57	333	250–300	112±14	119	270–350	19.3±3.5	19
	420–490	138±29	145	300–370	89.0±12.2	91	350–450	9.1±2.5	6
	490–570	60.0±13.6	66	370–480	67.0±14.2	75	450–650	5.0±1.6	5
	570–650	13.8±3.9	21	480–640	35.0±8.0	40	>650	4.4±1.6	5
	>650	3.6±1.5	2	640–800	10.0±2.7	16			
				>800	3.4±1.5	4			
$N_j = 3$–5, $N_b = 1$	200–250	305±34	300	150–175	93.4±10.7	87	150–180	13.5±3.1	28
	250–310	167±21	172	175–210	69.5±8.7	71	180–230	8.7±2.2	7
	310–380	103±16	98	210–270	52.8±6.8	63	230–350	6.2±1.6	9
	380–460	43.6±8.7	47	270–380	38.6±5.1	47	>350	3.5±1.0	3
	460–550	17.9±4.1	19	380–600	15.9±3.2	19			
	>550	4.0±1.1	4	>600	3.6±0.9	4			
$N_j = 3$–5, $N_b = 2$	200–250	91.1±22.0	97	130–160	42.4±7.5	53	130–200	6.8±2.3	9
	250–325	52.7±13.7	39	160–200	26.5±5.5	29	>200	2.9±1.1	6
	325–425	18.6±5.8	16	200–270	15.4±3.7	19			
	>425	4.5±1.9	11	270–370	5.5±1.7	11			
				>370	2.9±1.1	5			
$N_j \geq 6$, $N_b = 0$	200–280	50.8±8.9	56	160–200	38.5±6.2	44	160–200	12.1±2.9	12
	280–380	14.7±3.1	16	200–250	19.3±3.6	34	200–300	10.1±3.2	7
	>380	7.3±2.3	8	250–325	14.1±2.8	23	>300	4.5±1.7	2
				325–425	5.8±1.9	9			
				>425	2.3±0.8	4			
$N_j \geq 6$, $N_b = 1$	200–250	32.0±6.7	31	150–190	38.7±5.9	38	150–200	7.3±3.2	6
	250–325	14.7±3.1	23	190–250	21.1±3.5	21	200–300	5.1±2.4	5
	>325	4.8±1.5	11	250–350	10.5±1.9	13	>300	2.3±1.1	1
				>350	3.0±0.8	4			
$N_j \geq 6$, $N_b = 2$	200–250	12.0±4.3	15	130–170	41.0±7.0	54	130–200	10.6±6.0	10
	250–300	4.6±1.6	13	170–220	19.4±3.8	28	>200	4.7±2.9	2
	>300	2.8±1.0	6	220–300	10.4±2.1	8			
				>300	4.3±0.8	6			
$N_j \geq 3$, $N_b \geq 3$	200–280	16.1±6.2	16	125–175	31.9±11.4	17	>125	4.5±2.1	3
	>280	4.6±1.7	7	175–275	16.1±6.3	13			
				>275	6.1±2.4	1			

Table 2. Event yields, for estimated background and data, in the signal regions of the inclusive-M_{T2} search. The uncertainties are the quadratic sum of statistical and systematic uncertainties.
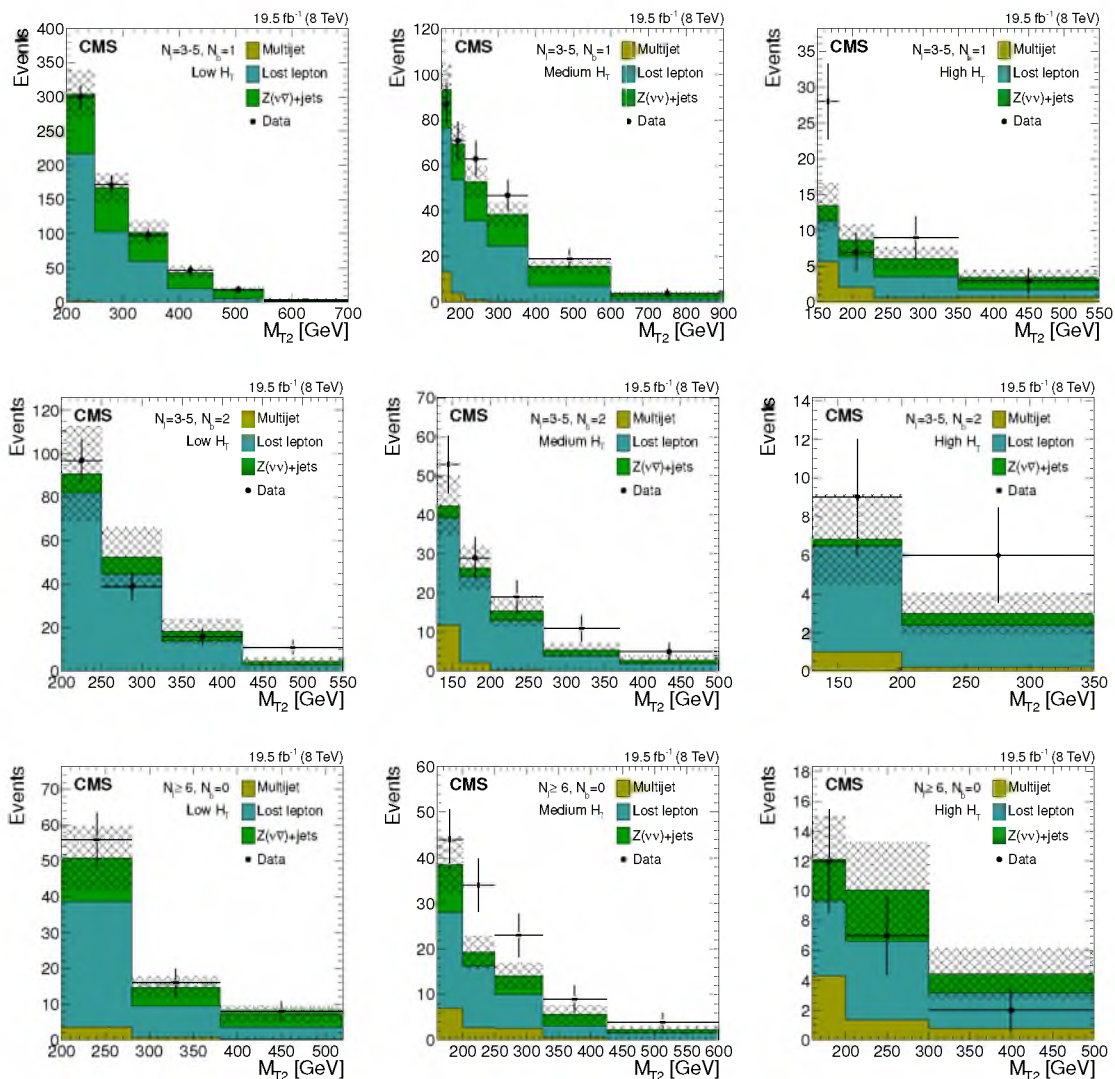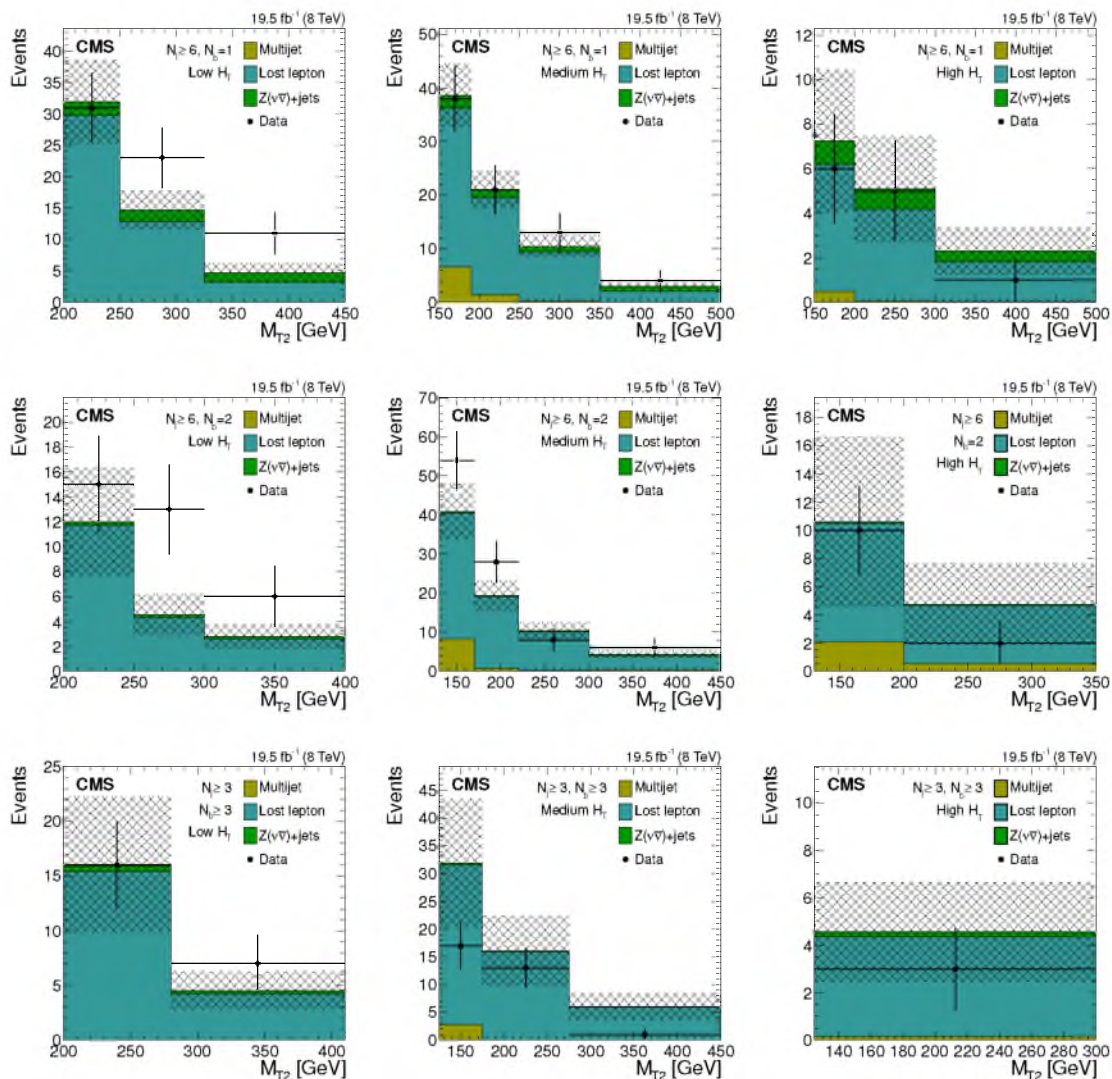
Figure 8. Distributions of the M_{T2} variable for the estimated background processes and for data. Plots are shown for events satisfying the low-H_T (left), the medium-H_T (middle), and the high-H_T (right) selections, and for different topological signal regions (N_j, N_b) of the inclusive-M_{T2} event selection. From top to bottom, these are ($3 \leq N_j \leq 5, N_b = 1$), ($3 \leq N_j \leq 5, N_b = 2$), ($N_j \geq 6, N_b = 0$). The uncertainties in each plot are drawn as the shaded band and do not include the uncertainty in the shape of the lost-lepton background.

signal region bin as:

$$\text{Pull} = \frac{N_{\text{obs}} - N_{\text{bkg}}}{\sqrt{\sigma_{\text{obs}}^2 + \sigma_{\text{bkg}}^2}}, \tag{7.1}$$

where N_{obs} is the observed number of events, σ_{obs} is its statistical uncertainty, and N_{bkg} is the background estimate with a total uncertainty of σ_{bkg}. After the average pull over all the signal regions is calculated, pseudo-experiments are used to evaluate the probability to observe an average at least as large as the average observed in data. The probability is found to be 11%. Thus, the data are found to be in agreement with the SM predictions within the uncertainties.

Figure 9. Distributions of the M_{T2} variable for the estimated background processes and for data. Plots are shown for events satisfying the low-H_T (left), the medium-H_T (middle), and the high-H_T (right) selections, and for different topological signal regions (N_j, N_b) of the inclusive-M_{T2} event selection. From top to bottom, these are ($N_j \geq 6$, $N_b = 1$), ($N_j \geq 6$, $N_b = 2$), ($N_j \geq 3$, $N_b \geq 3$). The uncertainties in each plot are drawn as the shaded band and do not include the uncertainty in the shape of the lost-lepton background.

In order to present the results in a compact manner, the yields of all M_{T2} bins that belong to the same topological region and that satisfy the same H_T selection are summed. The resulting sums are presented in figure 10.

7.2 Results for the M_{T2} Higgs analysis

For the M_{T2}-Higgs analysis, the observed numbers of events in data and the predicted background yields are summarized in table 3 for the two different selections in H_T. The background predictions and the data yields are shown for the different M_{bb} bins in figure 11

Figure 10. Event yields, for both estimated backgrounds and data, for the three H_T selections and all the topological signal regions of the inclusive-M_{T2} search. The uncertainties are drawn as the shaded band and do not include the uncertainty in the shape of the lost-lepton background.

Channel	Lost lepton	Z $(\nu\overline{\nu})$+jets	Total background	Data
Low-H_T	37.1 ± 9.0	6.9 ± 6.9	44.0 ± 11.3	55
High-H_T	64.8 ± 16.4	4.4 ± 4.4	69.2 ± 17.0	81

Table 3. Event yields for the W($\ell\nu$)+jets and $t\bar{t}$ +jets processes (i.e. the lost-lepton background), the Z $(\nu\overline{\nu})$+jets background, and data. Yields are shown for both the low- and the high-H_T selections of the M_{T2}-Higgs search. The lost-lepton background is estimated from data control samples, while the Z $(\nu\overline{\nu})$+jets is evaluated using simulation.

along with the distribution of events for a possible SUSY scenario. This scenario is based on gluino pair production in which one of the gluinos produces one h boson in its decay chain. More details about this signal scenario are provided in section 10.1.

8 Systematic uncertainties

A summary of the range-of-effect for each source of uncertainty relevant for the background prediction or signal efficiency is presented in table 4. While the systematic uncertainties in the background predictions have already been discussed in section 6, the dominant sources of systematic uncertainties in the selection efficiencies of signal events are described here.

The corrections for the differences observed between the signal simulation and data due to the jet energy scale and b-tagging efficiencies yield uncertainties in the signal yield
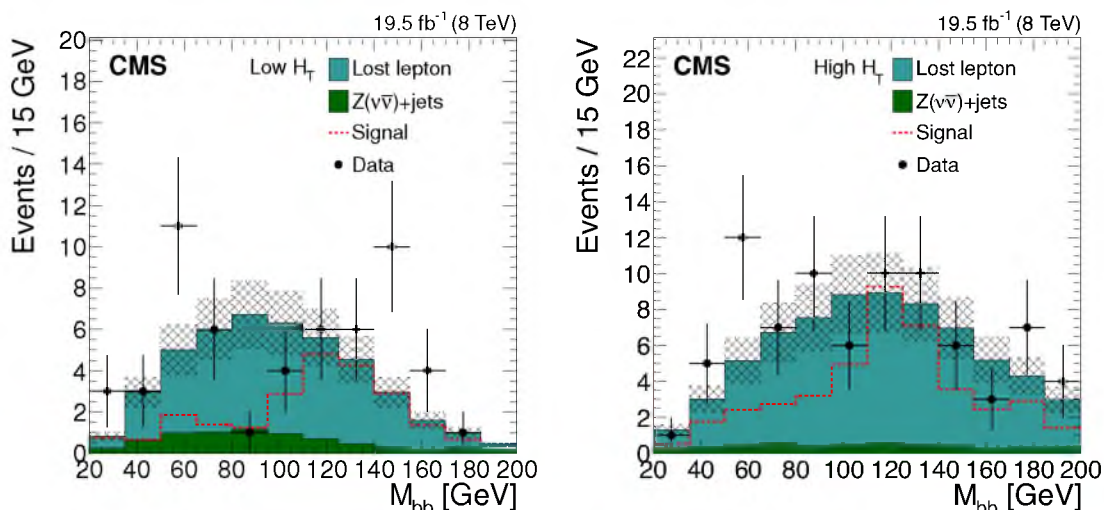
Figure 11. Distributions of the M_{bb} variable for the W($\ell\nu$)+jets and $t\bar{t}$ +jets processes (i.e. the lost-lepton background), the Z ($\nu\bar{\nu}$)+jets background, data, and a possible SUSY signal. The distributions are shown for both the low- (left) and the high-H_T (right) selections of the M_{T2}-Higgs search. The lost-lepton background is estimated from data control samples, while the Z ($\nu\bar{\nu}$)+jets is evaluated using simulation. The uncertainties in each plot are drawn as the shaded band and do not include the uncertainty in the shape of the lost-lepton background. The signal model consists of gluino pair production events with one of the two gluinos containing an h boson in its decay chain. For this model it is assumed $m_{\tilde{g}} = 750\,\text{GeV}$ and $m_{\tilde{\chi}_1^0} = 350\,\text{GeV}$.

of around 5%, but these uncertainties can become as large as 40% in kinematically extreme regions. The uncertainty associated with the corresponding correction to account for the p_T spectrum of the recoil system reaches a maximum of 20% for $p_T > 250\,\text{GeV}$. The systematic uncertainty associated with the parton distribution functions is evaluated following the prescription of the PDF4LHC group [59–63], and is found to have an effect of about 5%, increasing to a maximum of 15% for small splittings between the parent particle mass and the LSP mass. Additionally, uncertainties associated with the luminosity determination [64] and the trigger efficiency are included.

9 Statistical interpretation of the results

This section describes the statistical procedure used to interpret the observed event yields in order to set upper limits on the cross sections of potential signal processes. A test of the background-only and signal+background hypotheses is performed using a modified frequentist approach, often referred to as CL_s [65].

Signal regions are combined through a joint likelihood function. This function is constructed as the product of Poisson probabilities for each bin of N_j, N_b, H_T, and M_{T2}. The Poisson probabilities are functions of the number of observed events in each bin, n_i, and the predictions in each bin, λ_i, where i ranges from 1 to the number of bins, N_{bins}. The

Process	Source/Region	Effect	Shape
Multijet	$M_{\mathrm{T2}} < 200\,\mathrm{GeV}$	10–50%	—
	$M_{\mathrm{T2}} \geq 200\,\mathrm{GeV}$	50–100%	—
W($\ell\nu$)+jets and Top	Lost-lepton method (sys $\oplus$ stat)	10–65%	—
	b-tagging scale factor	—	x
	Jet energy scale	—	x
	Matching scale	—	x
	Renormalization and factorization scales	—	x
	System recoil modelling	—	x
Z ($\nu\bar{\nu}$)+jets	Systematics on $Z(\nu\bar{\nu})/\gamma$ ratio ($N_{\mathrm{b}} = 0\text{–}1$)	20–30%	—
	Systematics on 1b/0b ratio from $Z_{\ell\ell}$ ($N_{\mathrm{b}} = 1$)	10–75%	—
	Statistics from γ+jets data ($N_{\mathrm{b}} = 0\text{–}1$)	5–100%	—
	Simulation ($N_{\mathrm{b}} \geq 2$)	100%	—
Signal	Integrated luminosity	2.6%	—
	Trigger efficiency	1%	—
	Parton distribution functions	5–15%	—
	b-tagging scale factor	5–40%	x
	Jet energy scale	5–40%	x
	System recoil modelling	10–20%	x

Table 4. Summary of the different systematic uncertainties of the SM background predictions and of the signal efficiency. A given source of uncertainty can contribute differently depending on the search region, and the typical ranges of effect are shown. Sources of uncertainty that change the shape of the M_{T2} distributions in the inclusive-M_{T2} analysis or the shape of the M_{bb} distributions in the M_{T2}-Higgs search are marked with a cross in the last column.

likelihood function is given by

$$\mathcal{L} = \prod_{i=1}^{N_{\mathrm{bins}}} \frac{\lambda_i^{n_i} \mathrm{e}^{-\lambda_i}}{n_i!}.$$ (9.1)

The prediction in each bin is a sum over the signal and background contributions:

$$\lambda_i = \mu\, s_i + \sum_{j=1}^{N_{\mathrm{bkg}}} b_{ij},$$ (9.2)

where b_{ij} is the background prediction in bin i for background source j, and s_i is the signal prediction in bin i, scaled by the signal-strength modifier μ to test other values of the signal production cross section, $\sigma = \mu\sigma_{\mathrm{sig}}$, with σ_{sig} the nominal cross section for the signal model under consideration.

The uncertainties are handled by introducing nuisance parameters θ. The signal and background expectations, therefore, become dependent on N_{sys} nuisance parameters θ_m, where $m = 1 \ldots N_{\mathrm{sys}}$, i.e. $s = s(\theta_m)$ and $b = b(\theta_m)$. All sources of uncertainties are

taken to be either 100%-correlated (positively or negatively) or uncorrelated (independent), whichever is found to be appropriate. Incorporating the nuisance parameters, the likelihood function becomes:

$$\mathcal{L}(\text{data}|\mu,\theta) = \text{Poisson}(\text{data}|\mu\, s(\theta) + b(\theta))p(\theta), \qquad (9.3)$$

where $p(\theta)$ is the probability density function associated with the given systematic uncertainty. In this equation, $\mathcal{L}(\text{data}|\mu,\theta)$ is the likelihood function for data for a given value of μ and θ.

In order to test the compatibility of the data with the background-only and signal+background hypotheses, a test statistic q_μ [66] is constructed starting from the profile-likelihood ratio:

$$q_\mu = -2\ln\frac{\mathcal{L}(\text{data}|\mu,\hat{\theta}_\mu)}{\mathcal{L}(\text{data}|\hat{\mu},\hat{\theta})}, \qquad \text{with } 0 \leq \hat{\mu} \leq \mu, \qquad (9.4)$$

where "data" can be the actual data or the output of a pseudo-experiment. Both the denominator and numerator are maximized. In the numerator, the signal parameter strength μ remains fixed and the likelihood is maximized for only the nuisance parameters, whose values after the maximization are denoted $\hat{\theta}_\mu$. In the denominator, the likelihood is maximized with respect to both μ and θ, and $\hat{\mu}$ and $\hat{\theta}$ are the values for which $\mathcal{L}$ is maximal. The lower constraint $0 \leq \hat{\mu}$ is imposed as the signal strength cannot be negative, while the upper constraint guarantees a one-sided confidence interval (this means that upward fluctuations of data are not considered as evidence against the signal hypothesis). The value of the test statistic for the actual observation is denoted as q_μ^{obs}. This test statistic was chosen by the LHC Higgs Combination Group [67].

To set limits, probabilities to observe an outcome at least as signal-like as the one observed are calculated for the null (background-only) hypothesis H_0 and for the test (signal+background) hypothesis H_1, for a given value of the signal-strength modifier μ, as:

$$\begin{aligned} \text{CL}_{\text{s+b}}(\mu) &= P(q_\mu \geq q_\mu^{\text{obs}}|H_1), \\ \text{CL}_{\text{b}}(\mu) &= P(q_\mu \geq q_\mu^{\text{obs}}|H_0). \end{aligned} \qquad (9.5)$$

The CL_{s} quantity is then defined as the ratio of these probabilities:

$$\text{CL}_{\text{s}}(\mu) = \frac{\text{CL}_{\text{s+b}}(\mu)}{\text{CL}_{\text{b}}(\mu)}. \qquad (9.6)$$

In the modified frequentist approach, the value of $\text{CL}_{\text{s}}(\mu)$ is required to be less than or equal to α in order to declare a $(1-\alpha)$ CL exclusion. We set 95% CL limits on the signal cross section by finding the value of μ for which $\text{CL}_{\text{s}}(\mu) = 0.05$.

In practice, the probability distributions of the background-only and the signal+background hypotheses are determined from distributions of the test statistic constructed from pseudo-experiments. Once the ensembles of pseudo-experiments for the two hypotheses are generated, the observed CL_{s} limit is calculated from these distributions and the actual observation of the test statistic q_μ^{obs}. The expected CL_{s} limit is calculated by replacing q_μ^{obs} by the expected median from the distribution of the background-only hypothesis. Further details on the procedure employed to compute the limits on the signal production cross section are given in ref. [67].

10 Exclusion limits

The 95% CL upper limits on signal production cross sections are computed following the CL_s formulation described in section 9, using the results presented in section 7 and the systematic uncertainties summarized in section 8.

10.1 Exclusion limits on simplified models

In this section, we interpret the results of our search in terms of simplified models [26], which allow the exclusion potential of the data to be examined in the context of a large variety of models.

The following list describes the simplified models that are probed and the corresponding subsets of signal regions from the inclusive-M_{T2} search that are used to set the limits:

- direct pair production of squarks with $\tilde{q} \to q\tilde{\chi}_1^0$. The topological regions that are used to probe this model are those defined by the selections $(N_j = 2, N_b = 0)$, $(N_j = 2, N_b \geq 1)$, $(3 \leq N_j \leq 5, N_b = 0)$, $(3 \leq N_j \leq 5, N_b = 1)$, and $(N_j \geq 6, N_b = 0)$. Exclusions limits are shown in figure 12 (upper left) for two scenarios: one assumes that the first two generations of squarks ($\tilde{u}_L$, $\tilde{u}_R$, $\tilde{d}_L$, $\tilde{d}_R$, $\tilde{c}_L$, $\tilde{c}_R$, $\tilde{s}_L$, $\tilde{s}_R$) are degenerate and light; the other requires that only one light-flavour squark be kinematically accessible.

- direct pair production of bottom squarks with $\tilde{b} \to b\tilde{\chi}_1^0$. The signal regions that are used are those defined by $(N_j = 2, N_b \geq 1)$, $(3 \leq N_j \leq 5, N_b = 1)$, and $(3 \leq N_j \leq 5, N_b = 2)$. The corresponding exclusion limits are shown in figure 12 (upper right).

- direct pair production of top squarks with $\tilde{t} \to t\tilde{\chi}_1^0$. The topological regions used to probe this model are those defined by $(3 \leq N_j \leq 5, N_b = 1)$, $(3 \leq N_j \leq 5, N_b = 2)$, $(N_j \geq 6, N_b = 1)$, $(N_j \geq 6, N_b = 2)$, and $(N_j \geq 3, N_b \geq 3)$. The corresponding exclusion limits are shown in figure 12 (bottom).

- gluino pair production with $\tilde{g} \to q\bar{q}\tilde{\chi}_1^0$. The topological regions used to probe this model are those defined by $(3 \leq N_j \leq 5, N_b = 0)$, $(3 \leq N_j \leq 5, N_b = 1)$, $(N_j \geq 6, N_b = 0)$, and $(N_j \geq 6, N_b = 1)$. The corresponding exclusion limits are shown in figure 13 (upper left).

- gluino pair production, with $\tilde{g} \to b\bar{b}\tilde{\chi}_1^0$. The topological regions used to probe this model are those defined by $(3 \leq N_j \leq 5, N_b = 1)$, $(3 \leq N_j \leq 5, N_b = 2)$, $(N_j \geq 6, N_b = 1)$, $(N_j \geq 6, N_b = 2)$, and $(N_j \geq 3, N_b \geq 3)$. The corresponding exclusion limits are shown in figure 13 (upper right).

- gluino pair production, with $\tilde{g} \to t\bar{t}\tilde{\chi}_1^0$. The topological regions used to probe this model are those defined by $(N_j \geq 6, N_b = 1)$, $(N_j \geq 6, N_b = 2)$, and $(N_j \geq 3, N_b \geq 3)$. The corresponding exclusion limits are shown in figure 13 (bottom).

All exclusion limits are obtained at NLO + next-to-the-leading-logarithm (NLL) order in α_s.

For the direct pair production of top squarks, the analysis is not sensitive to model points with $m_{\widetilde{t}} - m_{\widetilde{\chi}_1^0} = m_{\mathrm{t}}$, because the $\widetilde{\chi}_1^0$ is produced at rest in the top-squark frame.

For all the considered models, the observed limits are compatible within one standard deviation with the expected limits, with the exception of the limits on the direct pair production of top squarks with $\widetilde{t} \to t\widetilde{\chi}_1^0$, which are shown in figure 12 (bottom). A comparison between the background estimates obtained directly from simulation and those calculated from the data control samples suggests that the weaker-than-expected limits are not caused by an excess in the signal region, but rather by a downward fluctuation in the lost-lepton control sample, leading to a possible underestimate of the lost-lepton background. Considering the large number of data control samples (there are 81 lost-lepton control regions), the probability to observe a fluctuation as large as the one observed is $\sim$65%.

The results of the M_{T2}-Higgs search are used to probe the following model: gluino pair production with one gluino decaying via $\widetilde{g} \to q\overline{q}\widetilde{\chi}_2^0$, $\widetilde{\chi}_2^0 \to h\widetilde{\chi}_1^0$, and the other gluino decaying via $\widetilde{g} \to qq'\widetilde{\chi}_1^\pm$, $\widetilde{\chi}_1^\pm \to W^\pm\widetilde{\chi}_1^0$. In this scenario, the neutralino $\widetilde{\chi}_2^0$ and chargino $\widetilde{\chi}_1^\pm$ are assumed to be degenerate, with mass $m_{\widetilde{\chi}_2^0} = m_{\widetilde{\chi}_1^\pm} = m_{\widetilde{\chi}_1^0} + 200\,\mathrm{GeV}$. The corresponding exclusion limits are shown in figure 14.

10.2 Exclusion limit in the cMSSM/mSUGRA model

We also provide an interpretation of our results in terms of the cMSSM/mSUGRA model. The model has five free parameters: m_0, $m_{1/2}$, A_0, $\tan\beta$, and $\mathrm{sign}\,\mu$. In order to obtain an h boson mass of about $125\,\mathrm{GeV}$, the value $A_0 = -2\max(m_0, m_{1/2})$ is chosen, as proposed in ref. [68]. Furthermore, we choose $\mu > 0$ and $\tan\beta = 30$. Exclusion limits as a function of m_0 and $m_{1/2}$ are shown in figure 15. These limits are presented in figure 16 as a function of $m_{\widetilde{g}}$ and $m_{\widetilde{q}}$, where $m_{\widetilde{q}}$ is the average mass of the first-generation squarks.

In table 5, we summarize the exclusion limits from figures 12–15.

11 Summary

A search for supersymmetry (SUSY) in hadronic final states characterized by large values of unbalanced transverse momentum has been carried out using a sample of $\sqrt{s} = 8\,\mathrm{TeV}$ pp collisions. The data were collected by the CMS experiment at the CERN LHC and correspond to an integrated luminosity of $19.5\,\mathrm{fb}^{-1}$. An event selection based on the kinematic mass variable M_{T2} has been employed to reduce the background from standard model processes and to enhance the sensitivity of the search to a wide range of SUSY signatures.

Two related searches have been implemented. The first is an inclusive search based on several signal regions defined by the number of jets and b-tagged jets, the hadronic energy in the event, and the value of the M_{T2} variable. The second is a search for events that contain a Higgs boson in the decay chain of a heavy SUSY particle. Assuming that this boson decays to a bottom quark-antiquark pair in accordance with the branching fraction of the standard model Higgs boson, this category of events has been investigated to seek an excess at $125\,\mathrm{GeV}$ in the invariant mass distribution of the selected b-tagged jet pairs.
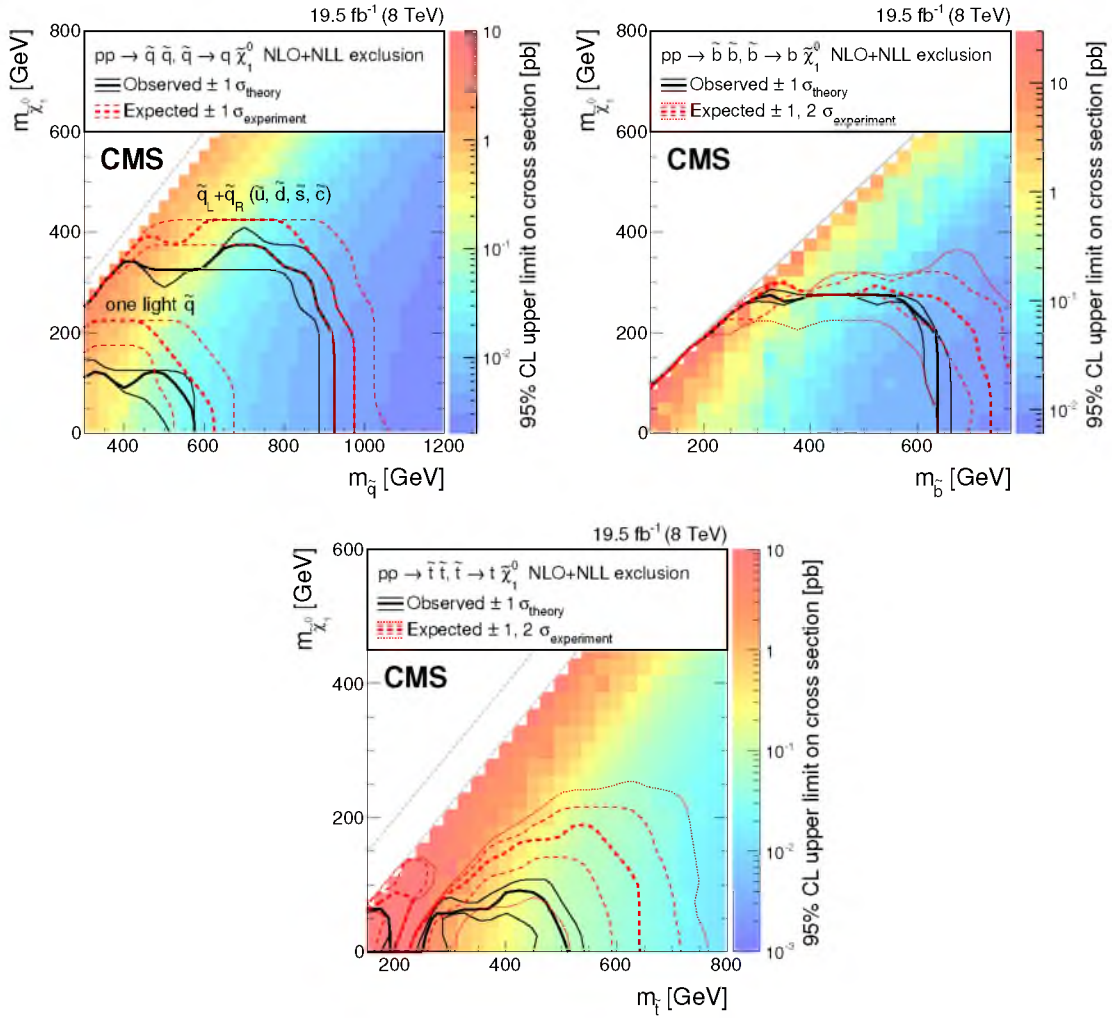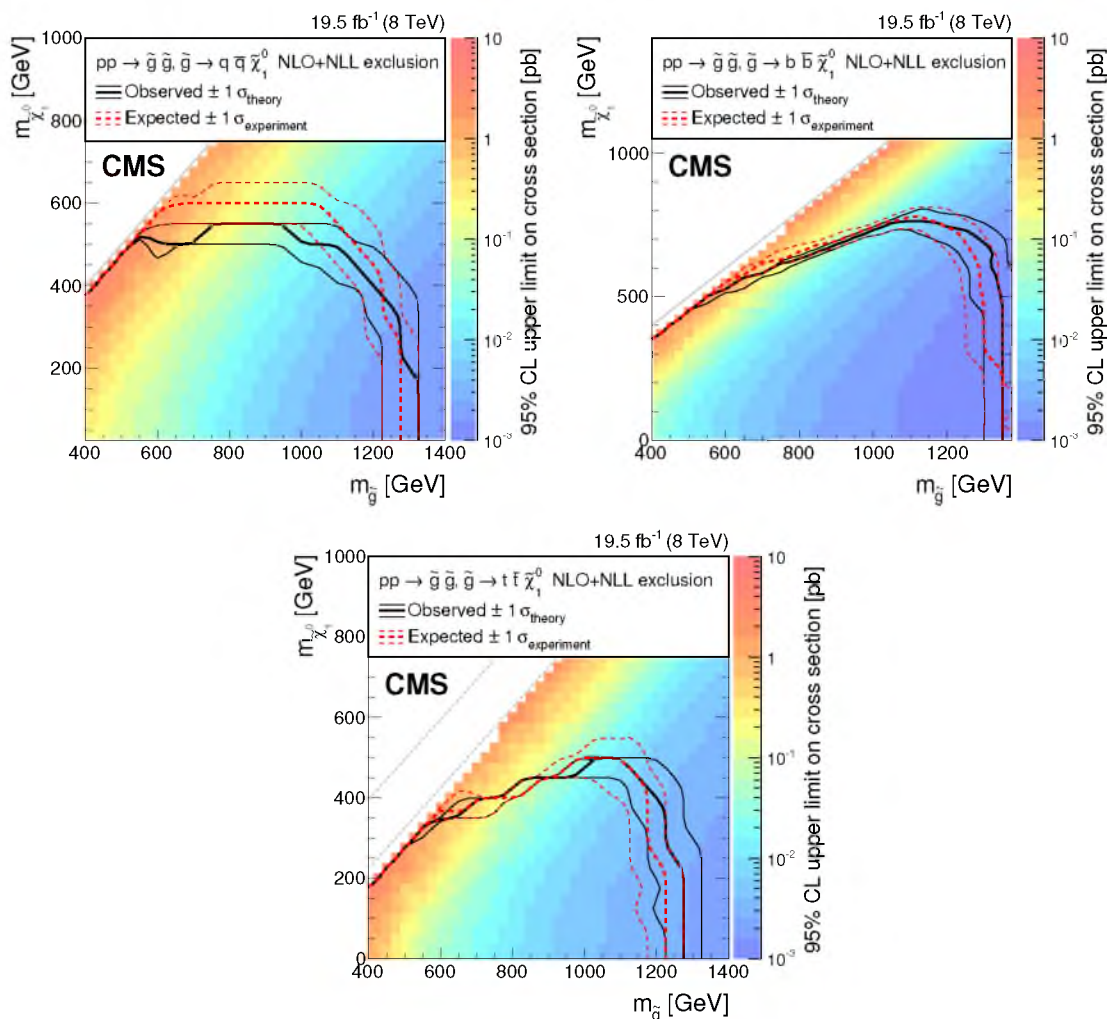
Figure 12. Exclusion limits at 95% CL for (upper left) direct squark production, (upper right) direct bottom-squark production, and (bottom) direct top-squark production. For the direct squark production, the upper set of curves corresponds to the scenario where the first two generations of squarks are degenerate and light, while the lower set corresponds to only one accessible light-flavour squark. For convenience, diagonal lines have been drawn corresponding to $m_{\tilde{\chi}_1^0} = m_{\tilde{q},\tilde{b},\tilde{t}}$ and $m_{\tilde{\chi}_1^0} = m_{\tilde{q},\tilde{b},\tilde{t}} - (m_W + m_b)$ where applicable.

No significant excess over the expected number of background events has been observed, and 95% confidence level exclusion limits on several SUSY simplified models and on the cMSSM/mSUGRA model have been derived. Mass limits have been conservatively derived using the theoretical signal cross sections reduced by one times their uncertainty $(-1\sigma_{\text{theory}})$. In the context of simplified models based on pair-produced gluinos, each decaying into a quark-antiquark pair and a lightest SUSY particle (LSP) via an off-shell squark, gluino masses have been probed up to 1225–1300 GeV depending on the squark flavour. For the direct pair production of the first- and second-generation squarks, each assumed to decay to a quark of the same flavour and a light LSP, masses below 875 GeV have been probed

Figure 13. Exclusion limits at 95% CL for gluino mediated (upper left) squark production, (upper right) bottom-squark production, and (bottom) top-squark production. For convenience, diagonal lines have been drawn corresponding to $m_{\widetilde{\chi}_1^0} = m_{\widetilde{g}}$ and $m_{\widetilde{\chi}_1^0} = m_{\widetilde{g}} - m_t$ where applicable.
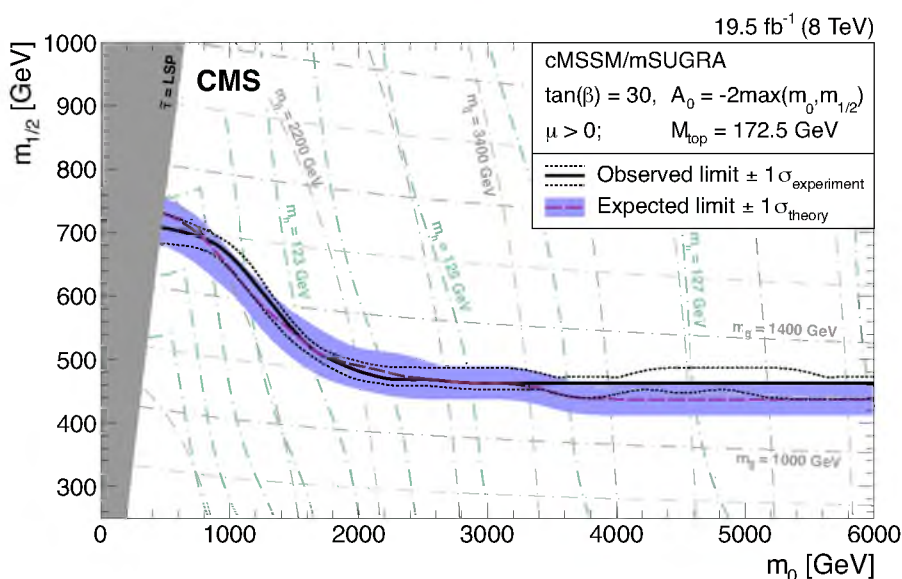
under the assumption of eight degenerate light squarks. If only a single squark is assumed to be light, this limit decreases to 520 GeV. For the direct production of third-generation squark pairs, each assumed to decay to a quark of the same flavour and a light LSP, masses up to 640 GeV for bottom squarks and 450 GeV for top squarks have been probed. In the cMSSM/mSUGRA scenario corresponding to $\tan\beta = 30$, $A_0 = -2\max(m_0, m_{1/2})$, and $\mu > 0$, absolute mass limits have been found to be: $m_{\widetilde{q}} > 1450\,\mathrm{GeV}$, $m_{\widetilde{g}} > 1150\,\mathrm{GeV}$, and $m_{\widetilde{q}} = m_{\widetilde{g}} > 1550\,\mathrm{GeV}$ when equal squark and gluino masses are assumed.

Acknowledgments

Figure 14. Exclusion limits at 95% CL for gluino pair production with one gluino decaying via $\widetilde{g} \rightarrow q\overline{q}\widetilde{\chi}_2^0$, $\widetilde{\chi}_2^0 \rightarrow h\widetilde{\chi}_1^0$, while the other gluino decays via $\widetilde{g} \rightarrow qq'\widetilde{\chi}_1^\pm$, $\widetilde{\chi}_1^\pm \rightarrow W^\pm\widetilde{\chi}_1^0$. For convenience, diagonal lines have been drawn corresponding to $m_{\widetilde{\chi}_1^0} = m_{\widetilde{g}}$ and $m_{\widetilde{\chi}_1^0} = m_{\widetilde{g}} - 200\,\text{GeV}$.

Figure 15. Exclusion limits at 95% CL as a function of m_0 and $m_{1/2}$ for the cMSSM/mSUGRA model with $\tan\beta = 30$, $A_0 = -2\max(m_0, m_{1/2})$, and $\mu > 0$. Here, $m_{\widetilde{q}}$ is the average mass of the first-generation squarks.

Figure 16. Exclusion limits at 95% CL as a function of $m_{\tilde{g}}$ and $m_{\tilde{q}}$ for the cMSSM/mSUGRA model with $\tan\beta = 30$, $A_0 = -2\max(m_0, m_{1/2})$, and $\mu > 0$. Here, $m_{\tilde{q}}$ is the average mass of the first-generation squarks.

Simplified model	Limit on parent particle mass at $m_{\widetilde{\chi}^0_1} = 0$	Best limit on LSP mass	Limit on mass splitting
Direct squark production			
Single light squark	$m_{\widetilde{q}} > 520\,\mathrm{GeV}$	$m_{\widetilde{\chi}^0_1} > 120\,\mathrm{GeV}$	$\Delta m(\widetilde{q}, \widetilde{\chi}^0_1) < 200\,\mathrm{GeV}$
8 degenerate light squarks	$m_{\widetilde{q}} > 875\,\mathrm{GeV}$	$m_{\widetilde{\chi}^0_1} > 325\,\mathrm{GeV}$	$\Delta m(\widetilde{q}, \widetilde{\chi}^0_1) < 50\,\mathrm{GeV}$
Bottom squark	$m_{\widetilde{b}} > 640\,\mathrm{GeV}$	$m_{\widetilde{\chi}^0_1} > 275\,\mathrm{GeV}$	$\Delta m(\widetilde{b}, \widetilde{\chi}^0_1) < 10\,\mathrm{GeV}$
Top squark			
$m_{\widetilde{t}} > m_{\mathrm{t}} + m_{\widetilde{\chi}^0_1}$	$m_{\widetilde{t}} > 450\,\mathrm{GeV}$	$m_{\widetilde{\chi}^0_1} > 60\,\mathrm{GeV}$	$\Delta m(\widetilde{t}, \widetilde{\chi}^0_1) < 230\,\mathrm{GeV}$
$m_{\widetilde{t}} < m_{\mathrm{t}} + m_{\widetilde{\chi}^0_1}$	$m_{\widetilde{t}} > 175\,\mathrm{GeV}$	$m_{\widetilde{\chi}^0_1} > 60\,\mathrm{GeV}$	$\Delta m(\widetilde{t}, \widetilde{\chi}^0_1) < 90\,\mathrm{GeV}$
Direct gluino production			
$\widetilde{g} \to q\overline{q}\widetilde{\chi}^0_1$	$m_{\widetilde{g}} > 1225\,\mathrm{GeV}$	$m_{\widetilde{\chi}^0_1} > 510\,\mathrm{GeV}$	$\Delta m(\widetilde{g}, \widetilde{\chi}^0_1) < 25\,\mathrm{GeV}$
$\widetilde{g} \to b\overline{b}\widetilde{\chi}^0_1$	$m_{\widetilde{g}} > 1300\,\mathrm{GeV}$	$m_{\widetilde{\chi}^0_1} > 740\,\mathrm{GeV}$	$\Delta m(\widetilde{g}, \widetilde{\chi}^0_1) < 50\,\mathrm{GeV}$
$\widetilde{g} \to t\overline{t}\widetilde{\chi}^0_1$	$m_{\widetilde{g}} > 1225\,\mathrm{GeV}$	$m_{\widetilde{\chi}^0_1} > 450\,\mathrm{GeV}$	$\Delta m(\widetilde{g}, \widetilde{\chi}^0_1) < 225\,\mathrm{GeV}$
$\widetilde{g}_1 \to q\overline{q}\widetilde{\chi}^0_2,\ \widetilde{\chi}^0_2 \to h\widetilde{\chi}^0_1,$ $\widetilde{g}_2 \to qq'\widetilde{\chi}^\pm_1,\ \chi^\pm_1 \to W^\pm\widetilde{\chi}^0_1$	$m_{\widetilde{g}} > 825\,\mathrm{GeV}$	$m_{\widetilde{\chi}^0_1} > 410\,\mathrm{GeV}$	$\Delta m(\widetilde{g}, \widetilde{\chi}^0_1) < 225\,\mathrm{GeV}$
cMSSM/mSUGRA model	Mass limit for $m_{\widetilde{q}} = m_{\widetilde{g}}$	Gluino mass limit	Squark mass limit
	$m_{\widetilde{g},\widetilde{q}} > 1550\,\mathrm{GeV}$	$m_{\widetilde{g}} > 1150\,\mathrm{GeV}$	$m_{\widetilde{q}} > 1450\,\mathrm{GeV}$

Table 5. Summary of observed mass limits (at 95% CL) for different SUSY simplified models and for the cMSSM/mSUGRA model. The limits quoted are the observed limits using the signal cross section minus one standard deviation (σ_{theory}) of its uncertainty. For the simplified models, the limit on the mass of the parent particle is quoted for $m_{\widetilde{\chi}^0_1} = 0$, while for the LSP the best limit on its mass is quoted. The best limit on the mass splitting between the parent particle mass and the LSP mass is also given. Finally, the absolute limits on the squark and gluino masses are quoted for the cMSSM/mSUGRA model.

References

[1] C.G. Lester and D.J. Summers, *Measuring masses of semi-invisibly decaying particles pair produced at hadron colliders*, *Phys. Lett.* **B 463** (1999) 99 [hep-ph/9906349] [INSPIRE].

[2] S.P. Martin, *A supersymmetry primer*, *Adv. Ser. Direct. High Energy Phys.* **21** (2010) 1 [hep-ph/9709356] [INSPIRE].

[3] CDF collaboration, T. Aaltonen et al., *Measurement of the top quark mass in the dilepton channel using m_{T2} at CDF*, *Phys. Rev.* **D 81** (2010) 031102 [arXiv:0911.2956] [INSPIRE].

[4] CMS collaboration, *Measurement of masses in the $t\bar{t}$ system by kinematic endpoints in pp collisions at $\sqrt{s} = 7$ TeV*, *Eur. Phys. J.* **C 73** (2013) 2494 [arXiv:1304.5783] [INSPIRE].

[5] CMS collaboration, *Search for supersymmetry in hadronic final states using M_{T2} in pp collisions at $\sqrt{s} = 7$ TeV*, *JHEP* **10** (2012) 018 [arXiv:1207.1798] [INSPIRE].

[6] CMS collaboration, *Searches for electroweak neutralino and chargino production in channels with Higgs, Z and W bosons in pp collisions at 8 TeV*, *Phys. Rev.* **D 90** (2014) 092007 [arXiv:1409.3168] [inSPIRE].

[7] ATLAS collaboration, *Search for direct slepton and gaugino production in final states with two leptons and missing transverse momentum with the ATLAS detector in pp collisions at $\sqrt{s} = 7$ TeV*, *Phys. Lett.* **B 718** (2013) 879 [arXiv:1208.2884] [inSPIRE].

[8] ATLAS collaboration, *Search for a heavy top-quark partner in final states with two leptons with the ATLAS detector at the LHC*, *JHEP* **11** (2012) 094 [arXiv:1209.4186] [inSPIRE].

[9] ATLAS collaboration, *Search for direct production of charginos and neutralinos in events with three leptons and missing transverse momentum in $\sqrt{s} = 8$ TeV pp collisions with the ATLAS detector*, *JHEP* **04** (2014) 169 [arXiv:1402.7029] [inSPIRE].

[10] ATLAS collaboration, *Search for direct top-squark pair production in final states with two leptons in pp collisions at $\sqrt{s} = 8$ TeV with the ATLAS detector*, *JHEP* **06** (2014) 124 [arXiv:1403.4853] [inSPIRE].

[11] ATLAS collaboration, *Search for direct production of charginos, neutralinos and sleptons in final states with two leptons and missing transverse momentum in pp collisions at $\sqrt{s} = 8$ TeV with the ATLAS detector*, *JHEP* **05** (2014) 071 [arXiv:1403.5294] [inSPIRE].

[12] ATLAS collaboration, *Search for the direct production of charginos, neutralinos and staus in final states with at least two hadronically decaying taus and missing transverse momentum in pp collisions at $\sqrt{s} = 8$ TeV with the ATLAS detector*, *JHEP* **1410** (2014) 96 [arXiv:1407.0350] [inSPIRE].

[13] ATLAS collaboration, *Search for top squark pair production in final states with one isolated lepton, jets and missing transverse momentum in $\sqrt{s} = 8$ TeV pp collisions with the ATLAS detector*, *JHEP* **11** (2014) 118 [arXiv:1407.0583] [inSPIRE].

[14] CMS collaboration, *Search for supersymmetry in hadronic final states with missing transverse energy using the variables α_T and b-quark multiplicity in pp collisions at $\sqrt{s} = 8$ TeV*, *Eur. Phys. J.* **C 73** (2013) 2568 [arXiv:1303.2985] [inSPIRE].

[15] CMS collaboration, *Search for gluino mediated bottom- and top-squark production in multijet final states in pp collisions at 8 TeV*, *Phys. Lett.* **B 725** (2013) 243 [arXiv:1305.2390] [inSPIRE].

[16] CMS collaboration, *Search for new physics in the multijet and missing transverse momentum final state in proton-proton collisions at $\sqrt{s} = 8$ TeV*, *JHEP* **06** (2014) 055 [arXiv:1402.4770] [inSPIRE].

[17] ATLAS collaboration, *Search for new phenomena in final states with large jet multiplicities and missing transverse momentum at $\sqrt{s} = 8$ TeV proton-proton collisions using the ATLAS experiment*, *JHEP* **10** (2013) 130 [arXiv:1308.1841] [inSPIRE].

[18] ATLAS collaboration, *Search for squarks and gluinos with the ATLAS detector in final states with jets and missing transverse momentum using $\sqrt{s} = 8$ TeV proton–proton collision data*, *JHEP* **09** (2014) 176 [arXiv:1405.7875] [inSPIRE].

[19] UA1 collaboration, G. Arnison et al., *Experimental observation of isolated large transverse energy electrons with associated missing energy at $\sqrt{s} = 540$ GeV*, *Phys. Lett.* **B 122** (1983) 103 [inSPIRE].

[20] CMS collaboration, *CMS technical design report, volume II: physics performance*, *J. Phys.* **G 34** (2007) 995 [inSPIRE].

[21] T. Sjöstrand, *The Lund Monte Carlo for e^+e^- jet physics*, *Comput. Phys. Commun.* **28** (1983) 229 [INSPIRE].

[22] T. Sjöstrand, S. Mrenna and P.Z. Skands, *PYTHIA 6.4 physics and manual*, *JHEP* **05** (2006) 026 [hep-ph/0603175] [INSPIRE].

[23] CMS collaboration, *The CMS experiment at the CERN LHC*, 2008 *JINST* **3** S08004 [INSPIRE].

[24] J. Alwall, M. Herquet, F. Maltoni, O. Mattelaer and T. Stelzer, *MadGraph 5: going beyond*, *JHEP* **06** (2011) 128 [arXiv:1106.0522] [INSPIRE].

[25] E. Re, *Single-top Wt-channel production matched with parton showers using the POWHEG method*, *Eur. Phys. J.* **C 71** (2011) 1547 [arXiv:1009.2450] [INSPIRE].

[26] LHC NEW PHYSICS WORKING GROUP collaboration, D. Alves et al., *Simplified models for LHC new physics searches*, *J. Phys.* **G 39** (2012) 105005 [arXiv:1105.2838] [INSPIRE].

[27] G.L. Kane, C.F. Kolda, L. Roszkowski and J.D. Wells, *Study of constrained minimal supersymmetry*, *Phys. Rev.* **D 49** (1994) 6173 [hep-ph/9312272] [INSPIRE].

[28] M. Muhlleitner, A. Djouadi and Y. Mambrini, *SDECAY: a Fortran code for the decays of the supersymmetric particles in the MSSM*, *Comput. Phys. Commun.* **168** (2005) 46 [hep-ph/0311167] [INSPIRE].

[29] B.C. Allanach, *SOFTSUSY: a program for calculating supersymmetric spectra*, *Comput. Phys. Commun.* **143** (2002) 305 [hep-ph/0104145] [INSPIRE].

[30] GEANT4 collaboration, S. Agostinelli et al., *GEANT4 — a simulation toolkit*, *Nucl. Instrum. Meth.* **A 506** (2003) 250 [INSPIRE].

[31] CMS collaboration, S. Abdullin, P. Azzi, F. Beaudette, P. Janot and A. Perrotta, *The fast simulation of the CMS detector at LHC*, *J. Phys. Conf. Ser.* **331** (2011) 032049 [INSPIRE].

[32] K. Melnikov and F. Petriello, *Electroweak gauge boson production at hadron colliders through $O(\alpha_s^2)$*, *Phys. Rev.* **D 74** (2006) 114017 [hep-ph/0609070] [INSPIRE].

[33] N. Kidonakis, *Next-to-next-to-leading soft-gluon corrections for the top quark cross section and transverse momentum distribution*, *Phys. Rev.* **D 82** (2010) 114030 [arXiv:1009.4935] [INSPIRE].

[34] A. Kulesza and L. Motyka, *Threshold resummation for squark-antisquark and gluino-pair production at the LHC*, *Phys. Rev. Lett.* **102** (2009) 111802 [arXiv:0807.2405] [INSPIRE].

[35] A. Kulesza and L. Motyka, *Soft gluon resummation for the production of gluino-gluino and squark-antisquark pairs at the LHC*, *Phys. Rev.* **D 80** (2009) 095004 [arXiv:0905.4749] [INSPIRE].

[36] W. Beenakker et al., *Soft-gluon resummation for squark and gluino hadroproduction*, *JHEP* **12** (2009) 041 [arXiv:0909.4418] [INSPIRE].

[37] W. Beenakker et al., *Squark and gluino hadroproduction*, *Int. J. Mod. Phys.* **A 26** (2011) 2637 [arXiv:1105.1110] [INSPIRE].

[38] M. Krämer et al., *Supersymmetry production cross sections in pp collisions at $\sqrt{s} = 7$ TeV*, arXiv:1206.2892 [INSPIRE].

[39] W. Beenakker, R. Hopker, M. Spira and P.M. Zerwas, *Squark and gluino production at hadron colliders*, *Nucl. Phys.* **B 492** (1997) 51 [hep-ph/9610490] [INSPIRE].

[40] CMS collaboration, *Particle-flow event reconstruction in CMS and performance for jets, taus and MET*, CMS-PAS-PFT-09-001 (2009).

[41] CMS collaboration, *Commissioning of the particle-flow event reconstruction with the first LHC collisions recorded in the CMS detector*, CMS-PAS-PFT-10-001 (2010).

[42] CMS Collaboration, *Electron reconstruction and identification at $\sqrt{s} = 7$ TeV*, CMS-PAS-EGM-10-004 (2010).

[43] CMS collaboration, *Performance of CMS muon reconstruction in pp collision events at $\sqrt{s} = 7$ TeV*, 2012 *JINST* **7** P10002 [arXiv:1206.4071] [INSPIRE].

[44] CMS collaboration, *Determination of jet energy calibration and transverse momentum resolution in CMS*, 2011 *JINST* **6** P11002 [arXiv:1107.4277] [INSPIRE].

[45] M. Cacciari, G.P. Salam and G. Soyez, *The anti-k_t jet clustering algorithm*, *JHEP* **04** (2008) 063 [arXiv:0802.1189] [INSPIRE].

[46] M. Cacciari and G.P. Salam, *Pileup subtraction using jet areas*, *Phys. Lett.* **B 659** (2008) 119 [arXiv:0707.1378] [INSPIRE].

[47] M. Cacciari, G.P. Salam and G. Soyez, *The catchment area of jets*, *JHEP* **04** (2008) 005 [arXiv:0802.1188] [INSPIRE].

[48] CMS collaboration, *Jet performance in pp collisions at 7 TeV*, CMS-PAS-JME-10-003 (2010).

[49] CMS collaboration, *Identification of b-quark jets with the CMS experiment*, 2013 *JINST* **8** P04013 [arXiv:1211.4462] [INSPIRE].

[50] CMS collaboration, *Performance of τ-lepton reconstruction and identification in CMS*, 2012 *JINST* **7** P01001 [arXiv:1109.6034] [INSPIRE].

[51] CMS collaboration, *Photon reconstruction and identification at $\sqrt{s} = 7$ TeV*, CMS-PAS-EGM-10-005 (2010).

[52] CMS collaboration, *Search for top-squark pair production in the single-lepton final state in pp collisions at $\sqrt{s} = 8$ TeV*, *Eur. Phys. J.* **C 73** (2013) 2677 [arXiv:1308.1586] [INSPIRE].

[53] CMS collaboration, *Missing transverse energy performance of the CMS detector*, 2011 *JINST* **6** P09001 [arXiv:1106.5048] [INSPIRE].

[54] ATLAS collaboration, *Observation of a new particle in the search for the standard model Higgs boson with the ATLAS detector at the LHC*, *Phys. Lett.* **B 716** (2012) 1 [arXiv:1207.7214] [INSPIRE].

[55] CMS collaboration, *Observation of a new boson at a mass of 125 GeV with the CMS experiment at the LHC*, *Phys. Lett.* **B 716** (2012) 30 [arXiv:1207.7235] [INSPIRE].

[56] CMS collaboration, *Measurement of the Inclusive W and Z production cross sections in pp collisions at $\sqrt{s} = 7$ TeV*, *JHEP* **10** (2011) 132 [arXiv:1107.4789] [INSPIRE].

[57] CMS collaboration, *First measurement of the cross section for top-quark pair production in proton-proton collisions at $\sqrt{s} = 7$ TeV*, *Phys. Lett.* **B 695** (2011) 424 [arXiv:1010.5994] [INSPIRE].

[58] S. Ask, M.A. Parker, T. Sandoval, M.E. Shea and W.J. Stirling, *Using $\gamma+$ jets production to calibrate the standard model $Z(\nu\nu)+$ jets background to new physics processes at the LHC*, *JHEP* **10** (2011) 058 [arXiv:1107.2803] [INSPIRE].

[59] S. Alekhin et al., *The PDF4LHC working group interim report*, arXiv:1101.0536 [INSPIRE].

[60] M. Botje et al., *The PDF4LHC working group interim recommendations*, arXiv:1101.0538 [INSPIRE].

[61] A.D. Martin, W.J. Stirling, R.S. Thorne and G. Watt, *Parton distributions for the LHC*, *Eur. Phys. J.* **C 63** (2009) 189 [arXiv:0901.0002] [INSPIRE].

[62] R.D. Ball et al., *A first unbiased global NLO determination of parton distributions and their uncertainties*, *Nucl. Phys.* **B 838** (2010) 136 [arXiv:1002.4407] [INSPIRE].

[63] H.-L. Lai et al., *New parton distributions for collider physics*, *Phys. Rev.* **D 82** (2010) 074024 [arXiv:1007.2241] [INSPIRE].

[64] CMS collaboration, *CMS Luminosity Based on Pixel Cluster Counting — Summer 2013 Update*, CMS-PAS-LUM-13-001 (2013).

[65] T. Junk, *Confidence level computation for combining searches with small statistics*, *Nucl. Instrum. Meth.* **A 434** (1999) 435 [hep-ex/9902006] [INSPIRE].

[66] G. Cowan, K. Cranmer, E. Gross and O. Vitells, *Asymptotic formulae for likelihood-based tests of new physics*, *Eur. Phys. J.* **C 71** (2011) 1554 [arXiv:1007.1727] [INSPIRE].

[67] ATLAS collaboration, *Procedure for the LHC Higgs boson search combination in summer 2011*, ATL-PHYS-PUB-2011-011 (2011).

[68] F. Brummer, S. Kraml and S. Kulkarni, *Anatomy of maximal stop mixing in the MSSM*, *JHEP* **08** (2012) 089 [arXiv:1204.5977] [INSPIRE].

The CMS collaboration

Yerevan Physics Institute, Yerevan, Armenia

V. Khachatryan, A.M. Sirunyan, A. Tumasyan

Institut für Hochenergiephysik der OeAW, Wien, Austria

W. Adam, T. Bergauer, M. Dragicevic, J. Erö, M. Friedl, R. Frühwirth[1], V.M. Ghete, C. Hartl, N. Hörmann, J. Hrubec, M. Jeitler[1], W. Kiesenhofer, V. Knünz, M. Krammer[1], I. Krätschmer, D. Liko, I. Mikulec, D. Rabady[2], B. Rahbaran, H. Rohringer, R. Schöfbeck, J. Strauss, W. Treberer-Treberspurg, W. Waltenberger, C.-E. Wulz[1]

National Centre for Particle and High Energy Physics, Minsk, Belarus

V. Mossolov, N. Shumeiko, J. Suarez Gonzalez

Universiteit Antwerpen, Antwerpen, Belgium

S. Alderweireldt, S. Bansal, T. Cornelis, E.A. De Wolf, X. Janssen, A. Knutsson, J. Lauwers, S. Luyckx, S. Ochesanu, R. Rougny, M. Van De Klundert, H. Van Haevermaet, P. Van Mechelen, N. Van Remortel, A. Van Spilbeeck

Vrije Universiteit Brussel, Brussel, Belgium

F. Blekman, S. Blyweert, J. D'Hondt, N. Daci, N. Heracleous, J. Keaveney, S. Lowette, M. Maes, A. Olbrechts, Q. Python, D. Strom, S. Tavernier, W. Van Doninck, P. Van Mulders, G.P. Van Onsem, I. Villella

Université Libre de Bruxelles, Bruxelles, Belgium

C. Caillol, B. Clerbaux, G. De Lentdecker, D. Dobur, L. Favart, A.P.R. Gay, A. Grebenyuk, A. Léonard, A. Mohammadi, L. Perniè[2], A. Randle-conde, T. Reis, T. Seva, L. Thomas, C. Vander Velde, P. Vanlaer, J. Wang, F. Zenoni

Ghent University, Ghent, Belgium

V. Adler, K. Beernaert, L. Benucci, A. Cimmino, S. Costantini, S. Crucy, S. Dildick, A. Fagot, G. Garcia, J. Mccartin, A.A. Ocampo Rios, D. Ryckbosch, S. Salva Diblen, M. Sigamani, N. Strobbe, F. Thyssen, M. Tytgat, E. Yazgan, N. Zaganidis

Université Catholique de Louvain, Louvain-la-Neuve, Belgium

S. Basegmez, C. Beluffi[3], G. Bruno, R. Castello, A. Caudron, L. Ceard, G.G. Da Silveira, C. Delaere, T. du Pree, D. Favart, L. Forthomme, A. Giammanco[4], J. Hollar, A. Jafari, P. Jez, M. Komm, V. Lemaitre, C. Nuttens, L. Perrini, A. Pin, K. Piotrzkowski, A. Popov[5], L. Quertenmont, M. Selvaggi, M. Vidal Marono, J.M. Vizan Garcia

Université de Mons, Mons, Belgium

N. Beliy, T. Caebergs, E. Daubie, G.H. Hammad

Centro Brasileiro de Pesquisas Fisicas, Rio de Janeiro, Brazil

W.L. Aldá Júnior, G.A. Alves, L. Brito, M. Correa Martins Junior, T. Dos Reis Martins, J. Molina, C. Mora Herrera, M.E. Pol, P. Rebello Teles

Universidade do Estado do Rio de Janeiro, Rio de Janeiro, Brazil

W. Carvalho, J. Chinellato[6], A. Custódio, E.M. Da Costa, D. De Jesus Damiao, C. De Oliveira Martins, S. Fonseca De Souza, H. Malbouisson, D. Matos Figueiredo, L. Mundim, H. Nogima, W.L. Prado Da Silva, J. Santaolalla, A. Santoro, A. Sznajder, E.J. Tonelli Manganote[6], A. Vilela Pereira

Universidade Estadual Paulista[a], Universidade Federal do ABC[b], São Paulo, Brazil

C.A. Bernardes[b], S. Dogra[a], T.R. Fernandez Perez Tomei[a], E.M. Gregores[b], P.G. Mercadante[b], S.F. Novaes[a], Sandra S. Padula[a]

Institute for Nuclear Research and Nuclear Energy, Sofia, Bulgaria

A. Aleksandrov, V. Genchev[2], R. Hadjiiska, P. Iaydjiev, A. Marinov, S. Piperov, M. Rodozov, S. Stoykova, G. Sultanov, M. Vutova

University of Sofia, Sofia, Bulgaria

A. Dimitrov, I. Glushkov, L. Litov, B. Pavlov, P. Petkov

Institute of High Energy Physics, Beijing, China

J.G. Bian, G.M. Chen, H.S. Chen, M. Chen, T. Cheng, R. Du, C.H. Jiang, R. Plestina[7], F. Romeo, J. Tao, Z. Wang

State Key Laboratory of Nuclear Physics and Technology, Peking University, Beijing, China

C. Asawatangtrakuldee, Y. Ban, Q. Li, S. Liu, Y. Mao, S.J. Qian, D. Wang, Z. Xu, W. Zou

Universidad de Los Andes, Bogota, Colombia

C. Avila, A. Cabrera, L.F. Chaparro Sierra, C. Florez, J.P. Gomez, B. Gomez Moreno, J.C. Sanabria

University of Split, Faculty of Electrical Engineering, Mechanical Engineering and Naval Architecture, Split, Croatia

N. Godinovic, D. Lelas, D. Polic, I. Puljak

University of Split, Faculty of Science, Split, Croatia

Z. Antunovic, M. Kovac

Institute Rudjer Boskovic, Zagreb, Croatia

V. Brigljevic, K. Kadija, J. Luetic, D. Mekterovic, L. Sudic

University of Cyprus, Nicosia, Cyprus

A. Attikis, G. Mavromanolakis, J. Mousa, C. Nicolaou, F. Ptochos, P.A. Razis

Charles University, Prague, Czech Republic

M. Bodlak, M. Finger, M. Finger Jr.[8]

Academy of Scientific Research and Technology of the Arab Republic of Egypt, Egyptian Network of High Energy Physics, Cairo, Egypt

Y. Assran[9], A. Ellithi Kamel[10], M.A. Mahmoud[11], A. Radi[12,13]

National Institute of Chemical Physics and Biophysics, Tallinn, Estonia

M. Kadastik, M. Murumaa, M. Raidal, A. Tiko

Department of Physics, University of Helsinki, Helsinki, Finland

P. Eerola, G. Fedi, M. Voutilainen

Helsinki Institute of Physics, Helsinki, Finland

J. Härkönen, V. Karimäki, R. Kinnunen, M.J. Kortelainen, T. Lampén, K. Lassila-Perini, S. Lehti, T. Lindén, P. Luukka, T. Mäenpää, T. Peltola, E. Tuominen, J. Tuominiemi, E. Tuovinen, L. Wendland

Lappeenranta University of Technology, Lappeenranta, Finland

J. Talvitie, T. Tuuva

DSM/IRFU, CEA/Saclay, Gif-sur-Yvette, France

M. Besancon, F. Couderc, M. Dejardin, D. Denegri, B. Fabbro, J.L. Faure, C. Favaro, F. Ferri, S. Ganjour, A. Givernaud, P. Gras, G. Hamel de Monchenault, P. Jarry, E. Locci, J. Malcles, J. Rander, A. Rosowsky, M. Titov

Laboratoire Leprince-Ringuet, Ecole Polytechnique, IN2P3-CNRS, Palaiseau, France

S. Baffioni, F. Beaudette, P. Busson, C. Charlot, T. Dahms, M. Dalchenko, L. Dobrzynski, N. Filipovic, A. Florent, R. Granier de Cassagnac, L. Mastrolorenzo, P. Miné, I.N. Naranjo, M. Nguyen, C. Ochando, G. Ortona, P. Paganini, S. Regnard, R. Salerno, J.B. Sauvan, Y. Sirois, C. Veelken, Y. Yilmaz, A. Zabi

Institut Pluridisciplinaire Hubert Curien, Université de Strasbourg, Université de Haute Alsace Mulhouse, CNRS/IN2P3, Strasbourg, France

J.-L. Agram[14], J. Andrea, A. Aubin, D. Bloch, J.-M. Brom, E.C. Chabert, C. Collard, E. Conte[14], J.-C. Fontaine[14], D. Gelé, U. Goerlach, C. Goetzmann, A.-C. Le Bihan, K. Skovpen, P. Van Hove

Centre de Calcul de l'Institut National de Physique Nucleaire et de Physique des Particules, CNRS/IN2P3, Villeurbanne, France

S. Gadrat

Université de Lyon, Université Claude Bernard Lyon 1, CNRS-IN2P3, Institut de Physique Nucléaire de Lyon, Villeurbanne, France

S. Beauceron, N. Beaupere, C. Bernet[7], G. Boudoul[2], E. Bouvier, S. Brochet, C.A. Carrillo Montoya, J. Chasserat, R. Chierici, D. Contardo[2], P. Depasse, H. El Mamouni, J. Fan, J. Fay, S. Gascon, M. Gouzevitch, B. Ille, T. Kurca, M. Lethuillier, L. Mirabito, S. Perries, J.D. Ruiz Alvarez, D. Sabes, L. Sgandurra, V. Sordini, M. Vander Donckt, P. Verdier, S. Viret, H. Xiao

Institute of High Energy Physics and Informatization, Tbilisi State University, Tbilisi, Georgia

Z. Tsamalaidze[8]

RWTH Aachen University, I. Physikalisches Institut, Aachen, Germany

C. Autermann, S. Beranek, M. Bontenackels, M. Edelhoff, L. Feld, A. Heister, K. Klein, A. Ostapchuk, M. Preuten, F. Raupach, J. Sammet, S. Schael, J.F. Schulte, H. Weber, B. Wittmer, V. Zhukov[5]

RWTH Aachen University, III. Physikalisches Institut A, Aachen, Germany

M. Ata, M. Brodski, E. Dietz-Laursonn, D. Duchardt, M. Erdmann, R. Fischer, A. Güth, T. Hebbeker, C. Heidemann, K. Hoepfner, D. Klingebiel, S. Knutzen, P. Kreuzer, M. Merschmeyer, A. Meyer, P. Millet, M. Olschewski, K. Padeken, P. Papacz, H. Reithler, S.A. Schmitz, L. Sonnenschein, D. Teyssier, S. Thüer, M. Weber

RWTH Aachen University, III. Physikalisches Institut B, Aachen, Germany

V. Cherepanov, Y. Erdogan, G. Flügge, H. Geenen, M. Geisler, W. Haj Ahmad, F. Hoehle, B. Kargoll, T. Kress, Y. Kuessel, A. Künsken, J. Lingemann[2], A. Nowack, I.M. Nugent, O. Pooth, A. Stahl

Deutsches Elektronen-Synchrotron, Hamburg, Germany

M. Aldaya Martin, I. Asin, N. Bartosik, J. Behr, U. Behrens, A.J. Bell, A. Bethani, K. Borras, A. Burgmeier, A. Cakir, L. Calligaris, A. Campbell, S. Choudhury, F. Costanza, C. Diez Pardos, G. Dolinska, S. Dooling, T. Dorland, G. Eckerlin, D. Eckstein, T. Eichhorn, G. Flucke, J. Garay Garcia, A. Geiser, P. Gunnellini, J. Hauk, M. Hempel[15], H. Jung, A. Kalogeropoulos, M. Kasemann, P. Katsas, J. Kieseler, C. Kleinwort, I. Korol, D. Krücker, W. Lange, J. Leonard, K. Lipka, A. Lobanov, W. Lohmann[15], B. Lutz, R. Mankel, I. Marfin[15], I.-A. Melzer-Pellmann, A.B. Meyer, G. Mittag, J. Mnich, A. Mussgiller, S. Naumann-Emme, A. Nayak, E. Ntomari, H. Perrey, D. Pitzl, R. Placakyte, A. Raspereza, P.M. Ribeiro Cipriano, B. Roland, E. Ron, M.Ö. Sahin, J. Salfeld-Nebgen, P. Saxena, T. Schoerner-Sadenius, M. Schröder, C. Seitz, S. Spannagel, A.D.R. Vargas Trevino, R. Walsh, C. Wissing

University of Hamburg, Hamburg, Germany

V. Blobel, M. Centis Vignali, A.R. Draeger, J. Erfle, E. Garutti, K. Goebel, M. Görner, J. Haller, M. Hoffmann, R.S. Höing, A. Junkes, H. Kirschenmann, R. Klanner, R. Kogler, J. Lange, T. Lapsien, T. Lenz, I. Marchesini, J. Ott, T. Peiffer, A. Perieanu, N. Pietsch, J. Poehlsen, T. Poehlsen, D. Rathjens, C. Sander, H. Schettler, P. Schleper, E. Schlieckau, A. Schmidt, M. Seidel, V. Sola, H. Stadie, G. Steinbrück, D. Troendle, E. Usai, L. Vanelderen, A. Vanhoefer

Institut für Experimentelle Kernphysik, Karlsruhe, Germany

C. Barth, C. Baus, J. Berger, C. Böser, E. Butz, T. Chwalek, W. De Boer, A. Descroix, A. Dierlamm, M. Feindt, F. Frensch, M. Giffels, A. Gilbert, F. Hartmann[2], T. Hauth, U. Husemann, I. Katkov[5], A. Kornmayer[2], P. Lobelle Pardo, M.U. Mozer, T. Müller, Th. Müller, A. Nürnberg, G. Quast, K. Rabbertz, S. Röcker, H.J. Simonis, F.M. Stober, R. Ulrich, J. Wagner-Kuhr, S. Wayand, T. Weiler, R. Wolf

Institute of Nuclear and Particle Physics (INPP), NCSR Demokritos, Aghia Paraskevi, Greece

G. Anagnostou, G. Daskalakis, T. Geralis, V.A. Giakoumopoulou, A. Kyriakis, D. Loukas, A. Markou, C. Markou, A. Psallidas, I. Topsis-Giotis

University of Athens, Athens, Greece

A. Agapitos, S. Kesisoglou, A. Panagiotou, N. Saoulidou, E. Stiliaris

University of Ioánnina, Ioánnina, Greece

X. Aslanoglou, I. Evangelou, G. Flouris, C. Foudas, P. Kokkas, N. Manthos, I. Papadopoulos, E. Paradas, J. Strologas

Wigner Research Centre for Physics, Budapest, Hungary

G. Bencze, C. Hajdu, P. Hidas, D. Horvath[16], F. Sikler, V. Veszpremi, G. Vesztergombi[17], A.J. Zsigmond

Institute of Nuclear Research ATOMKI, Debrecen, Hungary

N. Beni, S. Czellar, J. Karancsi[18], J. Molnar, J. Palinkas, Z. Szillasi

University of Debrecen, Debrecen, Hungary

A. Makovec, P. Raics, Z.L. Trocsanyi, B. Ujvari

National Institute of Science Education and Research, Bhubaneswar, India

S.K. Swain

Panjab University, Chandigarh, India

S.B. Beri, V. Bhatnagar, R. Gupta, U.Bhawandeep, A.K. Kalsi, M. Kaur, R. Kumar, M. Mittal, N. Nishu, J.B. Singh

University of Delhi, Delhi, India

Ashok Kumar, Arun Kumar, S. Ahuja, A. Bhardwaj, B.C. Choudhary, A. Kumar, S. Malhotra, M. Naimuddin, K. Ranjan, V. Sharma

Saha Institute of Nuclear Physics, Kolkata, India

S. Banerjee, S. Bhattacharya, K. Chatterjee, S. Dutta, B. Gomber, Sa. Jain, Sh. Jain, R. Khurana, A. Modak, S. Mukherjee, D. Roy, S. Sarkar, M. Sharan

Bhabha Atomic Research Centre, Mumbai, India

A. Abdulsalam, D. Dutta, V. Kumar, A.K. Mohanty[2], L.M. Pant, P. Shukla, A. Topkar

Tata Institute of Fundamental Research, Mumbai, India

T. Aziz, S. Banerjee, S. Bhowmik[19], R.M. Chatterjee, R.K. Dewanjee, S. Dugad, S. Ganguly, S. Ghosh, M. Guchait, A. Gurtu[20], G. Kole, S. Kumar, M. Maity[19], G. Majumder, K. Mazumdar, G.B. Mohanty, B. Parida, K. Sudhakar, N. Wickramage[21]

Institute for Research in Fundamental Sciences (IPM), Tehran, Iran

H. Bakhshiansohi, H. Behnamian, S.M. Etesami[22], A. Fahim[23], R. Goldouzian, M. Khakzad, M. Mohammadi Najafabadi, M. Naseri, S. Paktinat Mehdiabadi, F. Rezaei Hosseinabadi, B. Safarzadeh[24], M. Zeinali

University College Dublin, Dublin, Ireland

M. Felcini, M. Grunewald

INFN Sezione di Bari^a, Università di Bari^b, Politecnico di Bari^c, Bari, Italy

M. Abbrescia^{a,b}, C. Calabria^{a,b}, S.S. Chhibra^{a,b}, A. Colaleo^a, D. Creanza^{a,c}, N. De Filippis^{a,c}, M. De Palma^{a,b}, L. Fiore^a, G. Iaselli^{a,c}, G. Maggi^{a,c}, M. Maggi^a, S. My^{a,c}, S. Nuzzo^{a,b}, A. Pompili^{a,b}, G. Pugliese^{a,c}, R. Radogna^{a,b,2}, G. Selvaggi^{a,b}, A. Sharma^a, L. Silvestris^{a,2}, R. Venditti^{a,b}, P. Verwilligen^a

INFN Sezione di Bologna^a, Università di Bologna^b, Bologna, Italy

G. Abbiendi^a, A.C. Benvenuti^a, D. Bonacorsi^{a,b}, S. Braibant-Giacomelli^{a,b}, L. Brigliadori^{a,b}, R. Campanini^{a,b}, P. Capiluppi^{a,b}, A. Castro^{a,b}, F.R. Cavallo^a, G. Codispoti^{a,b}, M. Cuffiani^{a,b}, G.M. Dallavalle^a, F. Fabbri^a, A. Fanfani^{a,b}, D. Fasanella^{a,b}, P. Giacomelli^a, C. Grandi^a, L. Guiducci^{a,b}, S. Marcellini^a, G. Masetti^a, A. Montanari^a, F.L. Navarria^{a,b}, A. Perrotta^a, F. Primavera^{a,b}, A.M. Rossi^{a,b}, T. Rovelli^{a,b}, G.P. Siroli^{a,b}, N. Tosi^{a,b}, R. Travaglini^{a,b}

INFN Sezione di Catania^a, Università di Catania^b, CSFNSM^c, Catania, Italy

S. Albergo^{a,b}, G. Cappello^a, M. Chiorboli^{a,b}, S. Costa^{a,b}, F. Giordano^{a,c,2}, R. Potenza^{a,b}, A. Tricomi^{a,b}, C. Tuve^{a,b}

INFN Sezione di Firenze^a, Università di Firenze^b, Firenze, Italy

G. Barbagli^a, V. Ciulli^{a,b}, C. Civinini^a, R. D'Alessandro^{a,b}, E. Focardi^{a,b}, E. Gallo^a, S. Gonzi^{a,b}, V. Gori^{a,b}, P. Lenzi^{a,b}, M. Meschini^a, S. Paoletti^a, G. Sguazzoni^a, A. Tropiano^{a,b}

INFN Laboratori Nazionali di Frascati, Frascati, Italy

L. Benussi, S. Bianco, F. Fabbri, D. Piccolo

INFN Sezione di Genova^a, Università di Genova^b, Genova, Italy

R. Ferretti^{a,b}, F. Ferro^a, M. Lo Vetere^{a,b}, E. Robutti^a, S. Tosi^{a,b}

INFN Sezione di Milano-Bicocca^a, Università di Milano-Bicocca^b, Milano, Italy

M.E. Dinardo^{a,b}, S. Fiorendi^{a,b}, S. Gennai^{a,2}, R. Gerosa^{a,b,2}, A. Ghezzi^{a,b}, P. Govoni^{a,b}, M.T. Lucchini^{a,b,2}, S. Malvezzi^a, R.A. Manzoni^{a,b}, A. Martelli^{a,b}, B. Marzocchi^{a,b,2}, D. Menasce^a, L. Moroni^a, M. Paganoni^{a,b}, D. Pedrini^a, S. Ragazzi^{a,b}, N. Redaelli^a, T. Tabarelli de Fatis^{a,b}

INFN Sezione di Napoli^a, Università di Napoli 'Federico II'^{b}, Università della Basilicata (Potenza)^c, Università G. Marconi (Roma)^d, Napoli, Italy

S. Buontempo^a, N. Cavallo^{a,c}, S. Di Guida^{a,d,2}, F. Fabozzi^{a,c}, A.O.M. Iorio^{a,b}, L. Lista^a, S. Meola^{a,d,2}, M. Merola^a, P. Paolucci^{a,2}

INFN Sezione di Padova^a, Università di Padova^b, Università di Trento (Trento)^c, Padova, Italy

N. Bacchetta^a, M. Bellato^a, M. Biasotto^{a,25}, D. Bisello^{a,b}, A. Branca^{a,b}, R. Carlin^{a,b}, P. Checchia^a, M. Dall'Osso^{a,b}, M. Galanti^{a,b}, F. Gasparini^{a,b}, U. Gasparini^{a,b}, F. Gonella^a,

A. Gozzelino[a], M. Margoni[a,b], A.T. Meneguzzo[a,b], J. Pazzini[a,b], N. Pozzobon[a,b],
P. Ronchese[a,b], F. Simonetto[a,b], E. Torassa[a], M. Tosi[a,b], S. Vanini[a,b], S. Ventura[a],
P. Zotto[a,b], A. Zucchetta[a,b], G. Zumerle[a,b]

INFN Sezione di Pavia[a], Università di Pavia[b], Pavia, Italy
M. Gabusi[a,b], S.P. Ratti[a,b], V. Re[a], C. Riccardi[a,b], P. Salvini[a], P. Vitulo[a,b]

INFN Sezione di Perugia[a], Università di Perugia[b], Perugia, Italy
M. Biasini[a,b], G.M. Bilei[a], D. Ciangottini[a,b,2], L. Fanò[a,b], P. Lariccia[a,b], G. Mantovani[a,b],
M. Menichelli[a], A. Saha[a], A. Santocchia[a,b], A. Spiezia[a,b,2]

INFN Sezione di Pisa[a], Università di Pisa[b], Scuola Normale Superiore di Pisa[c], Pisa, Italy
K. Androsov[a,26], P. Azzurri[a], G. Bagliesi[a], J. Bernardini[a], T. Boccali[a], G. Broccolo[a,c],
R. Castaldi[a], M.A. Ciocci[a,26], R. Dell'Orso[a], S. Donato[a,c,2], F. Fiori[a,c], L. Foà[a,c],
A. Giassi[a], M.T. Grippo[a,26], F. Ligabue[a,c], T. Lomtadze[a], L. Martini[a,b], A. Messineo[a,b],
C.S. Moon[a,27], F. Palla[a,2], A. Rizzi[a,b], A. Savoy-Navarro[a,28], A.T. Serban[a], P. Spagnolo[a],
P. Squillacioti[a,26], R. Tenchini[a], G. Tonelli[a,b], A. Venturi[a], P.G. Verdini[a], C. Vernieri[a,c]

INFN Sezione di Roma[a], Università di Roma[b], Roma, Italy
L. Barone[a,b], F. Cavallari[a], G. D'imperio[a,b], D. Del Re[a,b], M. Diemoz[a], C. Jorda[a],
E. Longo[a,b], F. Margaroli[a,b], P. Meridiani[a], F. Micheli[a,b,2], G. Organtini[a,b], R. Paramatti[a],
S. Rahatlou[a,b], C. Rovelli[a], F. Santanastasio[a,b], L. Soffi[a,b], P. Traczyk[a,b,2]

INFN Sezione di Torino[a], Università di Torino[b], Università del Piemonte Orientale (Novara)[c], Torino, Italy
N. Amapane[a,b], R. Arcidiacono[a,c], S. Argiro[a,b], M. Arneodo[a,c], R. Bellan[a,b], C. Biino[a],
N. Cartiglia[a], S. Casasso[a,b,2], M. Costa[a,b], A. Degano[a,b], N. Demaria[a], L. Finco[a,b,2],
C. Mariotti[a], S. Maselli[a], E. Migliore[a,b], V. Monaco[a,b], M. Musich[a], M.M. Obertino[a,c],
L. Pacher[a,b], N. Pastrone[a], M. Pelliccioni[a], G.L. Pinna Angioni[a,b], A. Potenza[a,b],
A. Romero[a,b], M. Ruspa[a,c], R. Sacchi[a,b], A. Solano[a,b], A. Staiano[a], U. Tamponi[a]

INFN Sezione di Trieste[a], Università di Trieste[b], Trieste, Italy
S. Belforte[a], V. Candelise[a,b,2], M. Casarsa[a], F. Cossutti[a], G. Della Ricca[a,b], B. Gobbo[a],
C. La Licata[a,b], M. Marone[a,b], A. Schizzi[a,b], T. Umer[a,b], A. Zanetti[a]

Kangwon National University, Chunchon, Korea
S. Chang, A. Kropivnitskaya, S.K. Nam

Kyungpook National University, Daegu, Korea
D.H. Kim, G.N. Kim, M.S. Kim, D.J. Kong, S. Lee, Y.D. Oh, H. Park, A. Sakharov,
D.C. Son

Chonbuk National University, Jeonju, Korea
T.J. Kim, M.S. Ryu

Chonnam National University, Institute for Universe and Elementary Particles, Kwangju, Korea
J.Y. Kim, D.H. Moon, S. Song

Korea University, Seoul, Korea

S. Choi, D. Gyun, B. Hong, M. Jo, H. Kim, Y. Kim, B. Lee, K.S. Lee, S.K. Park, Y. Roh

Seoul National University, Seoul, Korea

H.D. Yoo

University of Seoul, Seoul, Korea

M. Choi, J.H. Kim, I.C. Park, G. Ryu

Sungkyunkwan University, Suwon, Korea

Y. Choi, Y.K. Choi, J. Goh, D. Kim, E. Kwon, J. Lee, I. Yu

Vilnius University, Vilnius, Lithuania

A. Juodagalvis

National Centre for Particle Physics, Universiti Malaya, Kuala Lumpur, Malaysia

J.R. Komaragiri, M.A.B. Md Ali

Centro de Investigacion y de Estudios Avanzados del IPN, Mexico City, Mexico

E. Casimiro Linares, H. Castilla-Valdez, E. De La Cruz-Burelo, I. Heredia-de La Cruz, A. Hernandez-Almada, R. Lopez-Fernandez, A. Sanchez-Hernandez

Universidad Iberoamericana, Mexico City, Mexico

S. Carrillo Moreno, F. Vazquez Valencia

Benemerita Universidad Autonoma de Puebla, Puebla, Mexico

I. Pedraza, H.A. Salazar Ibarguen

Universidad Autónoma de San Luis Potosí, San Luis Potosí, Mexico

A. Morelos Pineda

University of Auckland, Auckland, New Zealand

D. Krofcheck

University of Canterbury, Christchurch, New Zealand

P.H. Butler, S. Reucroft

National Centre for Physics, Quaid-I-Azam University, Islamabad, Pakistan

A. Ahmad, M. Ahmad, Q. Hassan, H.R. Hoorani, W.A. Khan, T. Khurshid, M. Shoaib

National Centre for Nuclear Research, Swierk, Poland

H. Bialkowska, M. Bluj, B. Boimska, T. Frueboes, M. Górski, M. Kazana, K. Nawrocki, K. Romanowska-Rybinska, M. Szleper, P. Zalewski

Institute of Experimental Physics, Faculty of Physics, University of Warsaw, Warsaw, Poland

G. Brona, K. Bunkowski, M. Cwiok, W. Dominik, K. Doroba, A. Kalinowski, M. Konecki, J. Krolikowski, M. Misiura, M. Olszewski

Laboratório de Instrumentação e Física Experimental de Partículas, Lisboa, Portugal

P. Bargassa, C. Beirão Da Cruz E Silva, P. Faccioli, P.G. Ferreira Parracho, M. Gallinaro, L. Lloret Iglesias, F. Nguyen, J. Rodrigues Antunes, J. Seixas, J. Varela, P. Vischia

Joint Institute for Nuclear Research, Dubna, Russia

P. Bunin, I. Golutvin, I. Gorbunov, V. Karjavin, V. Konoplyanikov, G. Kozlov, A. Lanev, A. Malakhov, V. Matveev[29], P. Moisenz, V. Palichik, V. Perelygin, M. Savina, S. Shmatov, S. Shulha, N. Skatchkov, V. Smirnov, A. Zarubin

Petersburg Nuclear Physics Institute, Gatchina (St. Petersburg), Russia

V. Golovtsov, Y. Ivanov, V. Kim[30], E. Kuznetsova, P. Levchenko, V. Murzin, V. Oreshkin, I. Smirnov, V. Sulimov, L. Uvarov, S. Vavilov, A. Vorobyev, An. Vorobyev

Institute for Nuclear Research, Moscow, Russia

Yu. Andreev, A. Dermenev, S. Gninenko, N. Golubev, M. Kirsanov, N. Krasnikov, A. Pashenkov, D. Tlisov, A. Toropin

Institute for Theoretical and Experimental Physics, Moscow, Russia

V. Epshteyn, V. Gavrilov, N. Lychkovskaya, V. Popov, I. Pozdnyakov, G. Safronov, S. Semenov, A. Spiridonov, V. Stolin, E. Vlasov, A. Zhokin

P.N. Lebedev Physical Institute, Moscow, Russia

V. Andreev, M. Azarkin[31], I. Dremin[31], M. Kirakosyan, A. Leonidov[31], G. Mesyats, S.V. Rusakov, A. Vinogradov

Skobeltsyn Institute of Nuclear Physics, Lomonosov Moscow State University, Moscow, Russia

A. Belyaev, E. Boos, M. Dubinin[32], L. Dudko, A. Ershov, A. Gribushin, V. Klyukhin, O. Kodolova, I. Lokhtin, S. Obraztsov, S. Petrushanko, V. Savrin, A. Snigirev

State Research Center of Russian Federation, Institute for High Energy Physics, Protvino, Russia

I. Azhgirey, I. Bayshev, S. Bitioukov, V. Kachanov, A. Kalinin, D. Konstantinov, V. Krychkine, V. Petrov, R. Ryutin, A. Sobol, L. Tourtchanovitch, S. Troshin, N. Tyurin, A. Uzunian, A. Volkov

University of Belgrade, Faculty of Physics and Vinca Institute of Nuclear Sciences, Belgrade, Serbia

P. Adzic[33], M. Ekmedzic, J. Milosevic, V. Rekovic

Centro de Investigaciones Energéticas Medioambientales y Tecnológicas (CIEMAT), Madrid, Spain

J. Alcaraz Maestre, C. Battilana, E. Calvo, M. Cerrada, M. Chamizo Llatas, N. Colino, B. De La Cruz, A. Delgado Peris, D. Domínguez Vázquez, A. Escalante Del Valle, C. Fernandez Bedoya, J.P. Fernández Ramos, J. Flix, M.C. Fouz, P. Garcia-Abia, O. Gonzalez Lopez, S. Goy Lopez, J.M. Hernandez, M.I. Josa, E. Navarro De Martino, A. Pérez-Calero Yzquierdo, J. Puerta Pelayo, A. Quintario Olmeda, I. Redondo, L. Romero, M.S. Soares

Universidad Autónoma de Madrid, Madrid, Spain

C. Albajar, J.F. de Trocóniz, M. Missiroli, D. Moran

Universidad de Oviedo, Oviedo, Spain

H. Brun, J. Cuevas, J. Fernandez Menendez, S. Folgueras, I. Gonzalez Caballero

Instituto de Física de Cantabria (IFCA), CSIC-Universidad de Cantabria, Santander, Spain

J.A. Brochero Cifuentes, I.J. Cabrillo, A. Calderon, J. Duarte Campderros, M. Fernandez, G. Gomez, A. Graziano, A. Lopez Virto, J. Marco, R. Marco, C. Martinez Rivero, F. Matorras, F.J. Munoz Sanchez, J. Piedra Gomez, T. Rodrigo, A.Y. Rodríguez-Marrero, A. Ruiz-Jimeno, L. Scodellaro, I. Vila, R. Vilar Cortabitarte

CERN, European Organization for Nuclear Research, Geneva, Switzerland

D. Abbaneo, E. Auffray, G. Auzinger, M. Bachtis, P. Baillon, A.H. Ball, D. Barney, A. Benaglia, J. Bendavid, L. Benhabib, J.F. Benitez, P. Bloch, A. Bocci, A. Bonato, O. Bondu, C. Botta, H. Breuker, T. Camporesi, G. Cerminara, S. Colafranceschi[34], M. D'Alfonso, D. d'Enterria, A. Dabrowski, A. David, F. De Guio, A. De Roeck, S. De Visscher, E. Di Marco, M. Dobson, M. Dordevic, B. Dorney, N. Dupont-Sagorin, A. Elliott-Peisert, G. Franzoni, W. Funk, D. Gigi, K. Gill, D. Giordano, M. Girone, F. Glege, R. Guida, S. Gundacker, M. Guthoff, J. Hammer, M. Hansen, P. Harris, J. Hegeman, V. Innocente, P. Janot, K. Kousouris, K. Krajczar, P. Lecoq, C. Lourenço, N. Magini, L. Malgeri, M. Mannelli, J. Marrouche, L. Masetti, F. Meijers, S. Mersi, E. Meschi, F. Moortgat, S. Morovic, M. Mulders, L. Orsini, L. Pape, E. Perez, A. Petrilli, G. Petrucciani, A. Pfeiffer, M. Pimiä, D. Piparo, M. Plagge, A. Racz, G. Rolandi[35], M. Rovere, H. Sakulin, C. Schäfer, C. Schwick, A. Sharma, P. Siegrist, P. Silva, M. Simon, P. Sphicas[36], D. Spiga, J. Steggemann, B. Stieger, M. Stoye, Y. Takahashi, D. Treille, A. Tsirou, G.I. Veres[17], N. Wardle, H.K. Wöhri, H. Wollny, W.D. Zeuner

Paul Scherrer Institut, Villigen, Switzerland

W. Bertl, K. Deiters, W. Erdmann, R. Horisberger, Q. Ingram, H.C. Kaestli, D. Kotlinski, U. Langenegger, D. Renker, T. Rohe

Institute for Particle Physics, ETH Zurich, Zurich, Switzerland

F. Bachmair, L. Bäni, L. Bianchini, M.A. Buchmann, B. Casal, N. Chanon, G. Dissertori, M. Dittmar, M. Donegà, M. Dünser, P. Eller, C. Grab, D. Hits, J. Hoss, W. Lustermann, B. Mangano, A.C. Marini, M. Marionneau, P. Martinez Ruiz del Arbol, M. Masciovecchio, D. Meister, N. Mohr, P. Musella, C. Nägeli[37], F. Nessi-Tedaldi, F. Pandolfi, F. Pauss, L. Perrozzi, M. Peruzzi, M. Quittnat, L. Rebane, M. Rossini, A. Starodumov[38], M. Takahashi, K. Theofilatos, R. Wallny, H.A. Weber

Universität Zürich, Zurich, Switzerland

C. Amsler[39], M.F. Canelli, V. Chiochia, A. De Cosa, A. Hinzmann, T. Hreus, B. Kilminster, C. Lange, B. Millan Mejias, J. Ngadiuba, D. Pinna, P. Robmann, F.J. Ronga, S. Taroni, M. Verzetti, Y. Yang

National Central University, Chung-Li, Taiwan

M. Cardaci, K.H. Chen, C. Ferro, C.M. Kuo, W. Lin, Y.J. Lu, R. Volpe, S.S. Yu

National Taiwan University (NTU), Taipei, Taiwan

P. Chang, Y.H. Chang, Y. Chao, K.F. Chen, P.H. Chen, C. Dietz, U. Grundler, W.-S. Hou, Y.F. Liu, R.-S. Lu, E. Petrakou, Y.M. Tzeng, R. Wilken

Chulalongkorn University, Faculty of Science, Department of Physics, Bangkok, Thailand

B. Asavapibhop, G. Singh, N. Srimanobhas, N. Suwonjandee

Cukurova University, Adana, Turkey

A. Adiguzel, M.N. Bakirci[40], S. Cerci[41], C. Dozen, I. Dumanoglu, E. Eskut, S. Girgis, G. Gokbulut, Y. Guler, E. Gurpinar, I. Hos, E.E. Kangal, A. Kayis Topaksu, G. Onengut[42], K. Ozdemir, S. Ozturk[40], A. Polatoz, D. Sunar Cerci[41], B. Tali[41], H. Topakli[40], M. Vergili, C. Zorbilmez

Middle East Technical University, Physics Department, Ankara, Turkey

I.V. Akin, B. Bilin, S. Bilmis, H. Gamsizkan[43], B. Isildak[44], G. Karapinar[45], K. Ocalan[46], S. Sekmen, U.E. Surat, M. Yalvac, M. Zeyrek

Bogazici University, Istanbul, Turkey

E.A. Albayrak[47], E. Gülmez, M. Kaya[48], O. Kaya[49], T. Yetkin[50]

Istanbul Technical University, Istanbul, Turkey

K. Cankocak, F.I. Vardarlı

National Scientific Center, Kharkov Institute of Physics and Technology, Kharkov, Ukraine

L. Levchuk, P. Sorokin

University of Bristol, Bristol, United Kingdom

J.J. Brooke, E. Clement, D. Cussans, H. Flacher, J. Goldstein, M. Grimes, G.P. Heath, H.F. Heath, J. Jacob, L. Kreczko, C. Lucas, Z. Meng, D.M. Newbold[51], S. Paramesvaran, A. Poll, T. Sakuma, S. Seif El Nasr-storey, S. Senkin, V.J. Smith

Rutherford Appleton Laboratory, Didcot, United Kingdom

K.W. Bell, A. Belyaev[52], C. Brew, R.M. Brown, D.J.A. Cockerill, J.A. Coughlan, K. Harder, S. Harper, E. Olaiya, D. Petyt, C.H. Shepherd-Themistocleous, A. Thea, I.R. Tomalin, T. Williams, W.J. Womersley, S.D. Worm

Imperial College, London, United Kingdom

M. Baber, R. Bainbridge, O. Buchmuller, D. Burton, D. Colling, N. Cripps, P. Dauncey, G. Davies, M. Della Negra, P. Dunne, W. Ferguson, J. Fulcher, D. Futyan, G. Hall, G. Iles, M. Jarvis, G. Karapostoli, M. Kenzie, R. Lane, R. Lucas[51], L. Lyons, A.-M. Magnan, S. Malik, B. Mathias, J. Nash, A. Nikitenko[38], J. Pela, M. Pesaresi, K. Petridis, D.M. Raymond, S. Rogerson, A. Rose, C. Seez, P. Sharp[†], A. Tapper, M. Vazquez Acosta, T. Virdee, S.C. Zenz

Brunel University, Uxbridge, United Kingdom

J.E. Cole, P.R. Hobson, A. Khan, P. Kyberd, D. Leggat, D. Leslie, I.D. Reid, P. Symonds, L. Teodorescu, M. Turner

Baylor University, Waco, U.S.A.

J. Dittmann, K. Hatakeyama, A. Kasmi, H. Liu, T. Scarborough, Z. Wu

The University of Alabama, Tuscaloosa, U.S.A.

O. Charaf, S.I. Cooper, C. Henderson, P. Rumerio

Boston University, Boston, U.S.A.

A. Avetisyan, T. Bose, C. Fantasia, P. Lawson, C. Richardson, J. Rohlf, J. St. John, L. Sulak

Brown University, Providence, U.S.A.

J. Alimena, E. Berry, S. Bhattacharya, G. Christopher, D. Cutts, Z. Demiragli, N. Dhingra, A. Ferapontov, A. Garabedian, U. Heintz, G. Kukartsev, E. Laird, G. Landsberg, M. Luk, M. Narain, M. Segala, T. Sinthuprasith, T. Speer, J. Swanson

University of California, Davis, Davis, U.S.A.

R. Breedon, G. Breto, M. Calderon De La Barca Sanchez, S. Chauhan, M. Chertok, J. Conway, R. Conway, P.T. Cox, R. Erbacher, M. Gardner, W. Ko, R. Lander, M. Mulhearn, D. Pellett, J. Pilot, F. Ricci-Tam, S. Shalhout, J. Smith, M. Squires, D. Stolp, M. Tripathi, S. Wilbur, R. Yohay

University of California, Los Angeles, U.S.A.

R. Cousins, P. Everaerts, C. Farrell, J. Hauser, M. Ignatenko, G. Rakness, E. Takasugi, V. Valuev, M. Weber

University of California, Riverside, Riverside, U.S.A.

K. Burt, R. Clare, J. Ellison, J.W. Gary, G. Hanson, J. Heilman, M. Ivova Rikova, P. Jandir, E. Kennedy, F. Lacroix, O.R. Long, A. Luthra, M. Malberti, M. Olmedo Negrete, A. Shrinivas, S. Sumowidagdo, S. Wimpenny

University of California, San Diego, La Jolla, U.S.A.

J.G. Branson, G.B. Cerati, S. Cittolin, R.T. D'Agnolo, A. Holzner, R. Kelley, D. Klein, J. Letts, I. Macneill, D. Olivito, S. Padhi, C. Palmer, M. Pieri, M. Sani, V. Sharma, S. Simon, M. Tadel, Y. Tu, A. Vartak, C. Welke, F. Würthwein, A. Yagil

University of California, Santa Barbara, Santa Barbara, U.S.A.

D. Barge, J. Bradmiller-Feld, C. Campagnari, T. Danielson, A. Dishaw, V. Dutta, K. Flowers, M. Franco Sevilla, P. Geffert, C. George, F. Golf, L. Gouskos, J. Incandela, C. Justus, N. Mccoll, J. Richman, D. Stuart, W. To, C. West, J. Yoo

California Institute of Technology, Pasadena, U.S.A.

A. Apresyan, A. Bornheim, J. Bunn, Y. Chen, J. Duarte, A. Mott, H.B. Newman, C. Pena, M. Pierini, M. Spiropulu, J.R. Vlimant, R. Wilkinson, S. Xie, R.Y. Zhu

Carnegie Mellon University, Pittsburgh, U.S.A.

V. Azzolini, A. Calamba, B. Carlson, T. Ferguson, Y. Iiyama, M. Paulini, J. Russ, H. Vogel, I. Vorobiev

University of Colorado at Boulder, Boulder, U.S.A.

J.P. Cumalat, W.T. Ford, A. Gaz, M. Krohn, E. Luiggi Lopez, U. Nauenberg, J.G. Smith, K. Stenson, S.R. Wagner

Cornell University, Ithaca, U.S.A.

J. Alexander, A. Chatterjee, J. Chaves, J. Chu, S. Dittmer, N. Eggert, N. Mirman, G. Nicolas Kaufman, J.R. Patterson, A. Ryd, E. Salvati, L. Skinnari, W. Sun, W.D. Teo, J. Thom, J. Thompson, J. Tucker, Y. Weng, L. Winstrom, P. Wittich

Fairfield University, Fairfield, U.S.A.

D. Winn

Fermi National Accelerator Laboratory, Batavia, U.S.A.

S. Abdullin, M. Albrow, J. Anderson, G. Apollinari, L.A.T. Bauerdick, A. Beretvas, J. Berryhill, P.C. Bhat, G. Bolla, K. Burkett, J.N. Butler, H.W.K. Cheung, F. Chlebana, S. Cihangir, V.D. Elvira, I. Fisk, J. Freeman, Y. Gao, E. Gottschalk, L. Gray, D. Green, S. Grünendahl, O. Gutsche, J. Hanlon, D. Hare, R.M. Harris, J. Hirschauer, B. Hooberman, S. Jindariani, M. Johnson, U. Joshi, B. Klima, B. Kreis, S. Kwan[†], J. Linacre, D. Lincoln, R. Lipton, T. Liu, J. Lykken, K. Maeshima, J.M. Marraffino, V.I. Martinez Outschoorn, S. Maruyama, D. Mason, P. McBride, P. Merkel, K. Mishra, S. Mrenna, S. Nahn, C. Newman-Holmes, V. O'Dell, O. Prokofyev, E. Sexton-Kennedy, S. Sharma, A. Soha, W.J. Spalding, L. Spiegel, L. Taylor, S. Tkaczyk, N.V. Tran, L. Uplegger, E.W. Vaandering, R. Vidal, A. Whitbeck, J. Whitmore, F. Yang

University of Florida, Gainesville, U.S.A.

D. Acosta, P. Avery, P. Bortignon, D. Bourilkov, M. Carver, D. Curry, S. Das, M. De Gruttola, G.P. Di Giovanni, R.D. Field, M. Fisher, I.K. Furic, J. Hugon, J. Konigsberg, A. Korytov, T. Kypreos, J.F. Low, K. Matchev, H. Mei, P. Milenovic[53], G. Mitselmakher, L. Muniz, A. Rinkevicius, L. Shchutska, M. Snowball, D. Sperka, J. Yelton, M. Zakaria

Florida International University, Miami, U.S.A.

S. Hewamanage, S. Linn, P. Markowitz, G. Martinez, J.L. Rodriguez

Florida State University, Tallahassee, U.S.A.

T. Adams, A. Askew, J. Bochenek, B. Diamond, J. Haas, S. Hagopian, V. Hagopian, K.F. Johnson, H. Prosper, V. Veeraraghavan, M. Weinberg

Florida Institute of Technology, Melbourne, U.S.A.

M.M. Baarmand, M. Hohlmann, H. Kalakhety, F. Yumiceva

University of Illinois at Chicago (UIC), Chicago, U.S.A.

M.R. Adams, L. Apanasevich, D. Berry, R.R. Betts, I. Bucinskaite, R. Cavanaugh, O. Evdokimov, L. Gauthier, C.E. Gerber, D.J. Hofman, P. Kurt, C. O'Brien, I.D. Sandoval Gonzalez, C. Silkworth, P. Turner, N. Varelas

The University of Iowa, Iowa City, U.S.A.

B. Bilki[54], W. Clarida, K. Dilsiz, M. Haytmyradov, J.-P. Merlo, H. Mermerkaya[55], A. Mestvirishvili, A. Moeller, J. Nachtman, H. Ogul, Y. Onel, F. Ozok[47], A. Penzo, R. Rahmat, S. Sen, P. Tan, E. Tiras, J. Wetzel, K. Yi

Johns Hopkins University, Baltimore, U.S.A.

B.A. Barnett, B. Blumenfeld, S. Bolognesi, D. Fehling, A.V. Gritsan, P. Maksimovic, C. Martin, M. Swartz

The University of Kansas, Lawrence, U.S.A.

P. Baringer, A. Bean, G. Benelli, C. Bruner, J. Gray, R.P. Kenny III, D. Majumder, M. Malek, M. Murray, D. Noonan, S. Sanders, J. Sekaric, R. Stringer, Q. Wang, J.S. Wood

Kansas State University, Manhattan, U.S.A.

I. Chakaberia, A. Ivanov, K. Kaadze, S. Khalil, M. Makouski, Y. Maravin, L.K. Saini, N. Skhirtladze, I. Svintradze

Lawrence Livermore National Laboratory, Livermore, U.S.A.

J. Gronberg, D. Lange, F. Rebassoo, D. Wright

University of Maryland, College Park, U.S.A.

A. Baden, A. Belloni, B. Calvert, S.C. Eno, J.A. Gomez, N.J. Hadley, R.G. Kellogg, T. Kolberg, Y. Lu, A.C. Mignerey, K. Pedro, A. Skuja, M.B. Tonjes, S.C. Tonwar

Massachusetts Institute of Technology, Cambridge, U.S.A.

A. Apyan, R. Barbieri, W. Busza, I.A. Cali, M. Chan, L. Di Matteo, G. Gomez Ceballos, M. Goncharov, D. Gulhan, M. Klute, Y.S. Lai, Y.-J. Lee, A. Levin, P.D. Luckey, C. Paus, D. Ralph, C. Roland, G. Roland, G.S.F. Stephans, K. Sumorok, D. Velicanu, J. Veverka, B. Wyslouch, M. Yang, M. Zanetti, V. Zhukova

University of Minnesota, Minneapolis, U.S.A.

B. Dahmes, A. Gude, S.C. Kao, K. Klapoetke, Y. Kubota, J. Mans, S. Nourbakhsh, N. Pastika, R. Rusack, A. Singovsky, N. Tambe, J. Turkewitz

University of Mississippi, Oxford, U.S.A.

J.G. Acosta, S. Oliveros

University of Nebraska-Lincoln, Lincoln, U.S.A.

E. Avdeeva, K. Bloom, S. Bose, D.R. Claes, A. Dominguez, R. Gonzalez Suarez, J. Keller, D. Knowlton, I. Kravchenko, J. Lazo-Flores, F. Meier, F. Ratnikov, G.R. Snow, M. Zvada

State University of New York at Buffalo, Buffalo, U.S.A.

J. Dolen, A. Godshalk, I. Iashvili, A. Kharchilava, A. Kumar, S. Rappoccio

Northeastern University, Boston, U.S.A.

G. Alverson, E. Barberis, D. Baumgartel, M. Chasco, A. Massironi, D.M. Morse, D. Nash, T. Orimoto, D. Trocino, R.-J. Wang, D. Wood, J. Zhang

Northwestern University, Evanston, U.S.A.

K.A. Hahn, A. Kubik, N. Mucia, N. Odell, B. Pollack, A. Pozdnyakov, M. Schmitt, S. Stoynev, K. Sung, M. Velasco, S. Won

University of Notre Dame, Notre Dame, U.S.A.

A. Brinkerhoff, K.M. Chan, A. Drozdetskiy, M. Hildreth, C. Jessop, D.J. Karmgard, N. Kellams, K. Lannon, S. Lynch, N. Marinelli, Y. Musienko[29], T. Pearson, M. Planer, R. Ruchti, G. Smith, N. Valls, M. Wayne, M. Wolf, A. Woodard

The Ohio State University, Columbus, U.S.A.

L. Antonelli, J. Brinson, B. Bylsma, L.S. Durkin, S. Flowers, A. Hart, C. Hill, R. Hughes, K. Kotov, T.Y. Ling, W. Luo, D. Puigh, M. Rodenburg, B.L. Winer, H. Wolfe, H.W. Wulsin

Princeton University, Princeton, U.S.A.

O. Driga, P. Elmer, J. Hardenbrook, P. Hebda, S.A. Koay, P. Lujan, D. Marlow, T. Medvedeva, M. Mooney, J. Olsen, P. Piroué, X. Quan, H. Saka, D. Stickland[2], C. Tully, J.S. Werner, A. Zuranski

University of Puerto Rico, Mayaguez, U.S.A.

E. Brownson, S. Malik, H. Mendez, J.E. Ramirez Vargas

Purdue University, West Lafayette, U.S.A.

V.E. Barnes, D. Benedetti, D. Bortoletto, M. De Mattia, L. Gutay, Z. Hu, M.K. Jha, M. Jones, K. Jung, M. Kress, N. Leonardo, D.H. Miller, N. Neumeister, B.C. Radburn-Smith, X. Shi, I. Shipsey, D. Silvers, A. Svyatkovskiy, F. Wang, W. Xie, L. Xu, J. Zablocki

Purdue University Calumet, Hammond, U.S.A.

N. Parashar, J. Stupak

Rice University, Houston, U.S.A.

A. Adair, B. Akgun, K.M. Ecklund, F.J.M. Geurts, W. Li, B. Michlin, B.P. Padley, R. Redjimi, J. Roberts, J. Zabel

University of Rochester, Rochester, U.S.A.

B. Betchart, A. Bodek, R. Covarelli, P. de Barbaro, R. Demina, Y. Eshaq, T. Ferbel, A. Garcia-Bellido, P. Goldenzweig, J. Han, A. Harel, O. Hindrichs, A. Khukhunaishvili, S. Korjenevski, G. Petrillo, D. Vishnevskiy

The Rockefeller University, New York, U.S.A.

R. Ciesielski, L. Demortier, K. Goulianos, C. Mesropian

Rutgers, The State University of New Jersey, Piscataway, U.S.A.

S. Arora, A. Barker, J.P. Chou, C. Contreras-Campana, E. Contreras-Campana, D. Duggan, D. Ferencek, Y. Gershtein, R. Gray, E. Halkiadakis, D. Hidas, S. Kaplan, A. Lath, S. Panwalkar, M. Park, R. Patel, S. Salur, S. Schnetzer, D. Sheffield, S. Somalwar, R. Stone, S. Thomas, P. Thomassen, M. Walker

University of Tennessee, Knoxville, U.S.A.

K. Rose, S. Spanier, A. York

Texas A&M University, College Station, U.S.A.

O. Bouhali[56], A. Castaneda Hernandez, R. Eusebi, W. Flanagan, J. Gilmore, T. Kamon[57], V. Khotilovich, V. Krutelyov, R. Montalvo, I. Osipenkov, Y. Pakhotin, A. Perloff, J. Roe, A. Rose, A. Safonov, I. Suarez, A. Tatarinov, K.A. Ulmer

Texas Tech University, Lubbock, U.S.A.

N. Akchurin, C. Cowden, J. Damgov, C. Dragoiu, P.R. Dudero, J. Faulkner, K. Kovitanggoon, S. Kunori, S.W. Lee, T. Libeiro, I. Volobouev

Vanderbilt University, Nashville, U.S.A.

E. Appelt, A.G. Delannoy, S. Greene, A. Gurrola, W. Johns, C. Maguire, Y. Mao, A. Melo, M. Sharma, P. Sheldon, B. Snook, S. Tuo, J. Velkovska

University of Virginia, Charlottesville, U.S.A.

M.W. Arenton, S. Boutle, B. Cox, B. Francis, J. Goodell, R. Hirosky, A. Ledovskoy, H. Li, C. Lin, C. Neu, J. Wood

Wayne State University, Detroit, U.S.A.

C. Clarke, R. Harr, P.E. Karchin, C. Kottachchi Kankanamge Don, P. Lamichhane, J. Sturdy

University of Wisconsin, Madison, U.S.A.

D.A. Belknap, D. Carlsmith, M. Cepeda, S. Dasu, L. Dodd, S. Duric, E. Friis, R. Hall-Wilton, M. Herndon, A. Hervé, P. Klabbers, A. Lanaro, C. Lazaridis, A. Levine, R. Loveless, A. Mohapatra, I. Ojalvo, T. Perry, G.A. Pierro, G. Polese, I. Ross, T. Sarangi, A. Savin, W.H. Smith, D. Taylor, C. Vuosalo, N. Woods

†: Deceased
1: Also at Vienna University of Technology, Vienna, Austria
2: Also at CERN, European Organization for Nuclear Research, Geneva, Switzerland
3: Also at Institut Pluridisciplinaire Hubert Curien, Université de Strasbourg, Université de Haute Alsace Mulhouse, CNRS/IN2P3, Strasbourg, France
4: Also at National Institute of Chemical Physics and Biophysics, Tallinn, Estonia
5: Also at Skobeltsyn Institute of Nuclear Physics, Lomonosov Moscow State University, Moscow, Russia
6: Also at Universidade Estadual de Campinas, Campinas, Brazil
7: Also at Laboratoire Leprince-Ringuet, Ecole Polytechnique, IN2P3-CNRS, Palaiseau, France
8: Also at Joint Institute for Nuclear Research, Dubna, Russia
9: Also at Suez University, Suez, Egypt
10: Also at Cairo University, Cairo, Egypt
11: Also at Fayoum University, El-Fayoum, Egypt
12: Also at British University in Egypt, Cairo, Egypt
13: Now at Ain Shams University, Cairo, Egypt
14: Also at Université de Haute Alsace, Mulhouse, France
15: Also at Brandenburg University of Technology, Cottbus, Germany
16: Also at Institute of Nuclear Research ATOMKI, Debrecen, Hungary

17: Also at Eötvös Loránd University, Budapest, Hungary
18: Also at University of Debrecen, Debrecen, Hungary
19: Also at University of Visva-Bharati, Santiniketan, India
20: Now at King Abdulaziz University, Jeddah, Saudi Arabia
21: Also at University of Ruhuna, Matara, Sri Lanka
22: Also at Isfahan University of Technology, Isfahan, Iran
23: Also at University of Tehran, Department of Engineering Science, Tehran, Iran
24: Also at Plasma Physics Research Center, Science and Research Branch, Islamic Azad University, Tehran, Iran
25: Also at Laboratori Nazionali di Legnaro dell'INFN, Legnaro, Italy
26: Also at Università degli Studi di Siena, Siena, Italy
27: Also at Centre National de la Recherche Scientifique (CNRS) - IN2P3, Paris, France
28: Also at Purdue University, West Lafayette, U.S.A.
29: Also at Institute for Nuclear Research, Moscow, Russia
30: Also at St. Petersburg State Polytechnical University, St. Petersburg, Russia
31: Also at National Research Nuclear University "Moscow Engineering Physics Institute" (MEPhI), Moscow, Russia
32: Also at California Institute of Technology, Pasadena, U.S.A.
33: Also at Faculty of Physics, University of Belgrade, Belgrade, Serbia
34: Also at Facoltà Ingegneria, Università di Roma, Roma, Italy
35: Also at Scuola Normale e Sezione dell'INFN, Pisa, Italy
36: Also at University of Athens, Athens, Greece
37: Also at Paul Scherrer Institut, Villigen, Switzerland
38: Also at Institute for Theoretical and Experimental Physics, Moscow, Russia
39: Also at Albert Einstein Center for Fundamental Physics, Bern, Switzerland
40: Also at Gaziosmanpasa University, Tokat, Turkey
41: Also at Adiyaman University, Adiyaman, Turkey
42: Also at Cag University, Mersin, Turkey
43: Also at Anadolu University, Eskisehir, Turkey
44: Also at Ozyegin University, Istanbul, Turkey
45: Also at Izmir Institute of Technology, Izmir, Turkey
46: Also at Necmettin Erbakan University, Konya, Turkey
47: Also at Mimar Sinan University, Istanbul, Istanbul, Turkey
48: Also at Marmara University, Istanbul, Turkey
49: Also at Kafkas University, Kars, Turkey
50: Also at Yildiz Technical University, Istanbul, Turkey
51: Also at Rutherford Appleton Laboratory, Didcot, United Kingdom
52: Also at School of Physics and Astronomy, University of Southampton, Southampton, United Kingdom
53: Also at University of Belgrade, Faculty of Physics and Vinca Institute of Nuclear Sciences, Belgrade, Serbia
54: Also at Argonne National Laboratory, Argonne, U.S.A.
55: Also at Erzincan University, Erzincan, Turkey
56: Also at Texas A&M University at Qatar, Doha, Qatar
57: Also at Kyungpook National University, Daegu, Korea